Cerebral Cortex, February 2016;26: 820–837

doi: 10.1093/cercor/bhv257
Advance Access Publication Date: 11 November 2015
Original Article

ORIGINAL ARTICLE

Thalamocortical Connections Drive Intracortical Activation of Functional Columns in the Mislaminated *Reeler* Somatosensory Cortex

Robin J. Wagener[1], Mirko Witte[1], Julien Guy[1], Nieves Mingo-Moreno[1,2], Sebastian Kügler[2,3] and Jochen F. Staiger[1,2]

[1]Institute for Neuroanatomy, Universitätsmedizin Göttingen, Georg-August-Universität Göttingen, 37075 Göttingen, Germany, [2]Center Nanoscale Microscopy and Molecular Physiology of the Brain (CNMPB), Göttingen, Germany and [3]Department of Neurology, Universitätsmedizin Göttingen, Georg-August-Universität Göttingen, 37075 Göttingen, Germany

Address correspondence to Dr Robin Wagener, Georg-August-Universität Göttingen, Zentrum Anatomie, Institut für Neuroanatomie, Kreuzbergring 40, D-37075 Göttingen, Germany. Email: robin.wagener@med.uni-goettingen.de, JanRobin.Wagener@unige.ch

Abstract

Neuronal wiring is key to proper neural information processing. Tactile information from the rodent's whiskers reaches the cortex via distinct anatomical pathways. The lemniscal pathway relays whisking and touch information from the ventral posteromedial thalamic nucleus to layer IV of the primary somatosensory "barrel" cortex. The disorganized neocortex of the *reeler* mouse is a model system that should severely compromise the ingrowth of thalamocortical axons (TCAs) into the cortex. Moreover, it could disrupt intracortical wiring. We found that neuronal intermingling within the *reeler* barrel cortex substantially exceeded previous descriptions, leading to the loss of layers. However, viral tracing revealed that TCAs still specifically targeted transgenically labeled spiny layer IV neurons. Slice electrophysiology and optogenetics proved that these connections represent functional synapses. In addition, we assessed intracortical activation via immediate-early-gene expression resulting from a behavioral exploration task. The cellular composition of activated neuronal ensembles suggests extensive similarities in intracolumnar information processing in the wild-type and *reeler* brains. We conclude that extensive ectopic positioning of neuronal partners can be compensated for by cell-autonomous mechanisms that allow for the establishment of proper connectivity. Thus, genetic neuronal fate seems to be of greater importance for correct cortical wiring than radial neuronal position.

Key words: c-fos, cortical layers, optogenetics, reelin, tracing

Introduction

For rodents, somatosensation plays a crucial role in the exploration of and orientation in the environment. They use the principal whiskers on their snout for object identification and discrimination (Guic-Robles et al. 1989; Brecht et al. 1997; Kleinfeld and Deschenes 2011). Peripheral information from the whisker pad reaches the cortex via (at least) 3 anatomically distinct pathways. These pathways are supposed to convey different aspects of the afferent information, such as whisking kinematics, contact timing, and touch information (Diamond et al. 2008). Thalamic projections from the dorsomedial section of the ventral

posteromedial nucleus of the thalamus (VPM) to rodent primary somatosensory cortex represent the most prominent stream of information. This "lemniscal" pathway conveys detailed whisking and touch information. The thalamocortical axons (TCAs) mainly project to layer IV of the primary somatosensory cortex. There they form elliptically shaped patches within the center of layer IV cellular aggregates called "barrels" and are able to functionally activate layer IV cells and, subsequently, the functional barrel-related columns (Woolsey and Van der Loos 1970; Bernardo and Woolsey 1987; Senft and Woolsey 1991; Wimmer et al. 2010). Neuronal activation can be visualized by immediate-early genes, such as the inducible transcription factor c-fos (Sagar et al. 1988; Staiger 2006; Barth 2007), which has been shown to be a suitable marker to resolve neuronal activation (i.e., elevated neuronal firing rates) in a cell-type-specific manner (Staiger et al. 2002; Yassin et al. 2010).

The *reeler* mouse is a homozygous reelin-deficient mutant that, due to its striking cortical phenotype, provides "a valuable experiment in nature" (Caviness et al. 1988) for key developmental mechanisms like neuronal migration (Hashimoto-Torii et al. 2008; Britto et al. 2011) or pathway formation (Harsan et al. 2013). For a long time, descriptions of the phenotype emphasized a relative inversion of cortical layers (Caviness and Sidman 1973; D'Arcangelo 2005). However, various features of the disorganized cortex indicated a more substantial defect of cortical layering (Caviness and Rakic 1978; Rakic and Caviness 1995). Work from our own laboratory as well as that from other groups confirmed and extended this view of a complex cellular disorganization: in the somatosensory cortex, neurons with different laminar characteristics are severely intermingled and become distributed all over the cortical thickness (Dekimoto et al. 2010; Wagener et al. 2010; Boyle et al. 2011). Nevertheless, tangential organization, and thus somatotopy within the primary somatosensory barrel cortex, seems to be maintained (Caviness 1976; Wagener et al. 2010; Guy et al. 2015). Previous studies proposed a preservation of the complex projection of TCAs into the (vertically) disorganized *reeler* cortex. However, these studies lacked identification of target cells for the TCAs and thus potentially underestimated the extent of miswiring (Steindler and Colwell 1976; Frost and Caviness 1980; Caviness and Frost 1983). As guidance of TCAs and synapse formation with their cortical partners are enormously complex processes (for review see Molnar et al. 2012), regular wiring of TCAs with extensively ectopic cortical target cells would demonstrate massive developmental plasticity. The ingrowth of TCAs into the cortex depends on genetically determined molecular cues as well as thalamic neurotransmission (O'Leary and Nakagawa 2002; Grove and Fukuchi-Shimogori 2003; Li et al. 2013). Interactions of thalamic axons with subplate cells seem to play an important role during thalamocortical pathfinding. Equivalent mechanisms have been postulated for the *reeler* cortex where thalamic fibers contact the superficially located "subplate," which consequently in *reeler* is called superplate (Molnar et al. 1998; Higashi et al. 2005).

Due to the increasing number of neurological syndromes that can be linked to defects in neuronal migration (Francis et al. 2006; Kerjan and Gleeson 2007; Valiente and Marin 2010), there is great interest in determining the consequences of ectopic neuronal positioning. Of particular interest is the wiring of these ectopically positioned cells, as well as the basic functional properties of cellular disorganized networks. In the present study, we used viral tracers, as well as channelrhodopsin-expressing viral vectors in combination with patch-clamp slice electrophysiology in a transgenic animal that allows for identification of neurons with a genetic layer IV characteristic. Thus, we were able to trace TCAs in the vicinity of clusters of ectopic "layer IV neurons" as well as test for functional synaptic contacts. Our results confirm and substantially extend the notion of intact thalamocortical contact formation in the disorganized *reeler* brain, namely, that terminal fields of TCAs overlap with clusters of neurons with genetic layer IV characteristics and appropriate synaptic markers. It was particularly important to verify functional synapses between TCAs and identified ectopic neurons with genetic layer IV characteristics. While the general question of thalamocortical wiring in the disorganized cortex has been a matter of research in previous studies (see above), very little was known about intracortical network activation in the disorganized cortex, as a measure of the integrity of intracortical wiring. Using a combination of molecular and classical histological techniques, we revealed that thalamocortical excitation led to a highly ordered activation of excitatory and inhibitory neuronal populations in the barrel-related column. Thus, we could demonstrate that basic principles of intracolumnar wiring and information processing seem largely unimpaired by cortical cellular intermingling (cf. Lodato et al. 2011). Taken together, our results imply that, despite misplacement of neurons due to migration defects, neuronal wiring into highly functional networks is still possible.

Materials and Methods

Animals

In total, 40 adult B6C3Fe mice (20 wt and 20 *reeler*) and 24 layer IV tdTomato mice (12 wt and 12 *reeler*) were used for the experiments. Mice were obtained from the central animal facility of the University Medical Center Goettingen. They were housed with a 12-h light/dark cycle, with food and water available ad libitum. All experimental procedures were approved by the local government.

Transgenic Animals

Scnn1a-Cre mice (full strain name: B6.Cg-Tg(Scnn1a-Cre)3Aibs/J; Stock Number: 009613; Jackson Laboratory) were crossed with heterozygous *reeler* animals (B6C3Fe *Reln* ±). The resulting Scnn1a-Cre *reeler* (±) were crossed again and animals homozygous for Scnn1a-Cre and heterozygous for *Reln* were chosen for further crossings. ROSA-Tomato-LSL mice (full strain name: B6;129S6-Gt(ROSA)26Sortm9(CAG-tdTomato)Hze/J; Stock number: 007905; Jackson Laboratory) were crossed with heterozygous *reeler* in the same way; the resulting strain was called ROSA-Tomato-LSL *reeler* (±). Crossing of Scnn1a-Tg3-Cre *reeler* (±) and Tomato-LSL *reeler* (±) resulted in layer IV-specific expression of tdTomato. Thus, the resulting line was called LIV^{tdTomato}, either wt or *reeler* (Guy et al. 2015). Heterozygous *reeler* animals were not used for experiments.

Enriched Environment

Eight LIV^{tdTomato} (4 wt and 4 *reeler*) and 32 B6C3Fe mice (16 wt and 16 *reeler*) were briefly anesthetized by intraperitoneal injection of ketamine (0.1 mg/g bodyweight) in order to clip certain sets of whiskers. On the right side of the snout, whiskers C1–3 remained intact, whereas B1–3 and D1–3 remained intact on the left side of the snout. The next day, the animals were placed in a large box (60 × 40 × 40 cm) containing a variety of natural and non-natural materials that were new to the animal (wood, a small styrofoam maze, cardboard, etc.). The mice explored the enriched environment for 2 h in the dark. Water and food were freely accessible. The animals were subsequently sacrificed by perfusion fixation.

Fixation and Tissue Processing

The adult animals for in situ hybridization (ISH) and immunohistochemistry (IHC) were perfused transcardially with 10 mL of 10%

sucrose, followed by 200 mL of 4% paraformaldehyde in 0.1 M phosphate buffer (PB), pH 7.4. Brains were dissected out and post-fixed for 2 h, then cryoprotected in 20% sucrose in 0.01 M phosphate-buffered saline (PBS) overnight at 4°C. Sectioning was done with a cryostat (CM 3050S; Leica) at 40 µm (ISH) or 50 µm (IHC) thickness. Most sections were cut in the standard coronal plane, but 4 LIV^{tdTomato} brains (2 wt and 2 *reeler*) were cut in the tangential plane (Welker and Woolsey 1974) (Fig. 2*C*,*D*).

Brightfield and Fluorescent Immunostaining

For a detailed description of the methods, see Wagener et al. (2010). In brief, the sections were rinsed in PB, Tris-buffer (TB), TB saline (TBS), and TBS-containing Triton X-100 (TBST) and lastly blocked with normal goat serum. They were incubated for 60 h at 6°C with the following primary antibodies: rabbit anti-c-Fos, sc52 (1:5000, Santa Cruz); mouse anti-GAD67, MAB5406 (1:20 000, Chemicon); mouse anti-SMI32, SMI32R (1:5000, Covance); mouse anti-PV, P-3088 (1:160 000, Sigma); rabbit anti-CR, 7696 (1:10 000, Swant); mouse anti-Calb, C-8666 (1:160 000, Sigma). For brightfield staining, the primary antibodies were detected with suitable biotinylated secondary antibodies (Vector Laboratories), diluted 1:200 in TBST and incubated for 2 h at room temperature. Afterward, peroxidase was coupled via an avidin–biotin complex (Vector Laboratories), diluted 1:200 in TBST. The chromogen was 0.015% 3,3′-diaminobenzidine (DAB; Sigma). To darken the staining reaction (in double labeling), 0.4% ammonium nickel sulfate (Fluka) was added. The staining reaction was initiated by the addition of hydrogen peroxide 0.006%. Color development was monitored by visual inspection with a stereomicroscope. For fluorescent staining, the primary antibodies were detected with suitable secondary antibodies conjugated to Alexa fluorophores (Invitrogen; 1:400). Fluorescent Nissl staining (NeuroTrace, Invitrogen) and DAPI staining (Molecular Probes) were performed according to the manufacturer's protocol. The sections were rinsed again and mounted in Aqua Poly Mount (Polysciences, Inc.).

In Situ Hybridization

ISH for the layer-specific markers *Ndnf* (also known as *A930038C07Rik*), *Rgs8*, *Rorb* (also known as *Rorbeta*), *Etv1* (also known as *Er81*), and *TC1460681* as well as for excitatory and inhibitory markers *Gad1* (also known as *GAD67*) and *Slc17a7* (also known as *vGlut1*) were performed with digoxigenin (DIG)-labeled cRNA probes. They were either generated directly from the appropriate plasmids containing full-length cDNA inserts specific for the respective laminar marker (Source BioScience), or in the case of *TC1460681*, *Gad1*, and *Slc17a7*, were first amplified from genomic cDNA with appropriate primers, cloned into the pCR-BluntII-TOPO Vector (Invitrogen), transfected into JM 109 competent *Escherichia coli* (Promega), amplified in overnight cultures, and purified with a purification kit (Qiagen). Order numbers of the full-length plasmids (Source BioScience): *Ndnf* (IRAVp968E1091D), *Rgs8* (IRAVp968E09162D), *Rorb* (IRAVp968D1267D), *Etv1* (IRAKp961E106Q). Primer Sequences: *TC1460681*, forward primer TCCT CAGAGAGTCAGTCCTTCC, reverse primer TACTGTGATCGGTTTT GGAGTG (Boyle et al. 2011); *Gad1*, forward primer GGCACGACT GTTTACGGAGC, reverse primer GCCTTGTCCCCGGTGTCATA; Slc17a7, forward primer CAGAGCCGGAGGAGATGA, reverse primer TTCCCTCAGAAACGCTGG, nested forward GCTGGCAGTGACGAAA GTGA, nested reverse TGAGAGGGAAAGAGGGCTGG. Plasmids underwent restriction digestion with the appropriate enzymes and subsequent in vitro transcription using a DIG RNA labeling kit (Roche). The sizes of the full-length probes were reduced to 350 base pairs via alkaline hydrolysis (0.2 M sodium carbonate and 0.2 M sodium bicarbonate at pH 10.2).

The thawed brain sections were rinsed 3 times (free floating) with 2× standard saline citrate (1 × SSC = 0.15 M NaCl, 0.015 M sodium citrate, pH 7.0) and pretreated for 15 min in hybridization buffer (HB; 50% formamide, 4 × SSC, 250 µg/mL denaturated salmon sperm DNA, 100 µg/mL tRNA, 5% dextransulfate and 1% Denhardt's solution) diluted 1:1 in 2× SSC at room temperature, followed by 1 h of incubation in pure HB at 55°C. Probe hybridization with DIG-labeled probes (200 ng/mL) was done overnight at the same temperature. Posthybridization washes were performed with 2 × SSC (2 × 15 min, at room temperature), 2 × SSC/50% formamide (15 min, at 65°C), 0.1 × SSC/50% formamide (15 min, at 65°C), 0.1 × SSC (2 × 15 min, at 65°C) and 0.01 M TBS, pH 7.4 (2 × 10 min, at room temperature). The probes were detected by anti-DIG Fab fragments conjugated to alkaline phosphatase (raised in sheep; Roche) diluted 1:1500 in TBS-containing blocking agent (Roche, at 4°C overnight). Hybridized probes were stained with nitroblue tetrazolium and 5-bromo-4-chloro-3-indolylphosphate (Roche). Development of the staining reaction was monitored with a stereo microscope. After the desired intensity was reached, the sections were rinsed again in TBS and mounted in Kaiser's glycerol gelatin (Merck).

Immunostaining Before ISH

The immunostaining was performed as described above using RNase-free material and buffers. The subsequent ISH was performed as described above as well.

Stereotactic Viral Vector Injection

The adeno-associated viral (AAV) vectors were custom manufactured by our "Viral Vectors Platform" of the DFG cluster of excellence CNMPB Goettingen. AAV-eGFP and AAV-Channelrhodopsin2(H134R)-eYFP consisted of AAV-2-ITRs, the human synapsin 1 gene promoter driving transgene expression, packaged in AAV-6 capsids (AAV2/6 eGFP; AAV2/6 ChR2-eYFP). For the anterograde tracing experiments, 4 adult B6C3Fe mice (2 wt and 2 *reeler*) and 8 adult LIV^{tdTomato} mice (4 wt and 4 *reeler*) were injected with the AAV2/6 eGFP. For the optogenetic/electrophysiology experiments, 6 postnatal (P) 21 LIV^{tdTomato} mice (3 wt and 3 *reeler*) were injected with the AAV2/6 ChR2-EYFP.

The animals were placed into a stereotactic frame (David Kopf Instruments) under constant anesthesia with ~3% isoflurane (analgesia: Lidocaine s.c., Metamizole p.o.). Two hundred nanoliters of the viral vector in sterile PBS was injected into the VPM; anterior – posterior: Bregma –1.7 mm; medial – lateral: ±1.75 mm; dorsal – ventral: –3.25 mm) via a Pressure System IIe (TooheySpritzer). The animals were kept alive for 2–3 weeks to allow for expression of the fluorescent protein and/or channelrhodopsin. For the tracing experiments, the native fluorescence signals were amplified via immunocytochemistry using a goat anti-GFP antibody (Abcam; 1:2000) to enhance the eGFP signal (secondary antibody: donkey anti-goat-Alexa 488; Invitrogen), while a rabbit anti-RFP (Rockland; 1:500) enhanced the tdTomato signal (secondary antibody: donkey anti-rabbit-Alexa 546; Invitrogen; immuno-protocol see above). Fluorochromes in the tissue of the optogenetic experiments were not enhanced. We checked all sections for retrogradely labeled, ChR2-expressing neurons in the cortex. No retrogradely labeled ChR2-expressing neurons were observed.

In Vitro Electrophysiology and Optogenetic Photostimulation

Two to three weeks after injection of the viral vector, the animals were anesthetized with isoflurane and sacrificed by decapitation. Thalamocortical slices of 300 µm thickness containing the primary somatosensory (barrel) cortex were sectioned with a vibratome (VT1200S; Leica). A cold (3–4°C) cutting solution containing the following (in mM) was used: 75 sucrose, 87 NaCl, 2.5 KCL, 0.5 $CaCl_2$, 7.0 $MgCl_2$, 26 $NaHCO_3$, 1.25 NaH_2PO_4, and 10 glucose continuously equilibrated with 95% O_2 and 5% CO_2, pH 7.4. The sections were preincubated for 0.5–1 h at 34°C and kept at room temperature for at least 30 min before recording.

Slices were transferred to a fixed-stage recording chamber in an upright microscope (Axio Examiner, Zeiss) and continuously perfused at a rate of 2 mL/min with extracellular solution (ACSF) of the following composition (in mM): 125 NaCl, 2.5 KCL, 2 $CaCl_2$, 1 $MgCl_2$, 26 $NaHCO_3$, 1.25 NaH_2PO_4 and 25 glucose, pH 7.4 when equilibrated with 95% O_2 and 5% CO_2. All experiments were performed at 32°C.

The barrel field was first visualized at low magnification (2.5×) under brightfield conditions. Afterward, expression of (YFP-tagged) channelrhodopsin was verified. Layer IV neurons were identified by tdTomato fluorescence with a 40× water immersion objective (Olympus, Germany). For whole-cell patch-clamp recordings, filamented borosilicate glass capillaries (Science Products, Hofheim, Germany) of 5–8 MΩ resistance were filled with (in mM): 135 K-gluconate, 5 KCL, 10 HEPES, 0.5 EGTA, 4 Mg-ATP, 0.3 Na-GTP, 10 phosphocreatine phosphate, and 0.3–0.5% biocytin. Membrane potentials were not corrected for the liquid junction potential of approximately –14 mV. Potentials were recorded using a SEC-05L amplifier (NPI Electronics, Tamm, Germany) in discontinuous current-clamp mode with a switching frequency of 50 kHz. The signals were filtered at 3 kHz and digitized at 10–25 kHz using a CED Power1401 (CED Limited, Cambridge, England). Data were collected, stored, and analyzed with Signal 5 software (CED Limited, Cambridge, England).

The passive and active properties of the recorded neurons were determined immediately after reaching whole-cell configuration by applying hyperpolarizing currents (10–50 pA) or depolarizing currents (10–200 pA) at resting membrane potential (Vrest), respectively. For assessing the connectivity of VPM neurons and layer IV cells in the barrel cortex of wt and *reeler* mice, full field photostimulation (diameter 100 µm) of ChR2-expressing VPM fibers was performed with a 473-nm laser light source (DL-473, Rapp OptoElectronik, Hamburg, Germany). The diode laser was coupled with a liquid fiber of 200 µm diameter to the epifluorescence path of the microscope and focused on the slice with the ×40 objective. Photostimulation was executed 3 times for the same illumination intensity (10–500 µW) and duration (1–10 ms) with an interval of at least 5 s. Latencies from stimulus to postsynaptic responses were measured using a laser intensity that was 9-fold higher that the intensity needed to elicit an EPSP in the first place in the recorded cell.

After recording, slices were fixed in 4% paraformaldehyde overnight at 4°C. For visualization of the biocytin-filled neurons, the sections were incubated with streptavidin-Alexa 633 (Invitrogen) 1:300.

Image Acquisition

Brightfield images (Figs 1, 3, 6 and 7) were acquired with an Axio Imager M2 (Zeiss) controlled by a Neurolucida system (Version11;

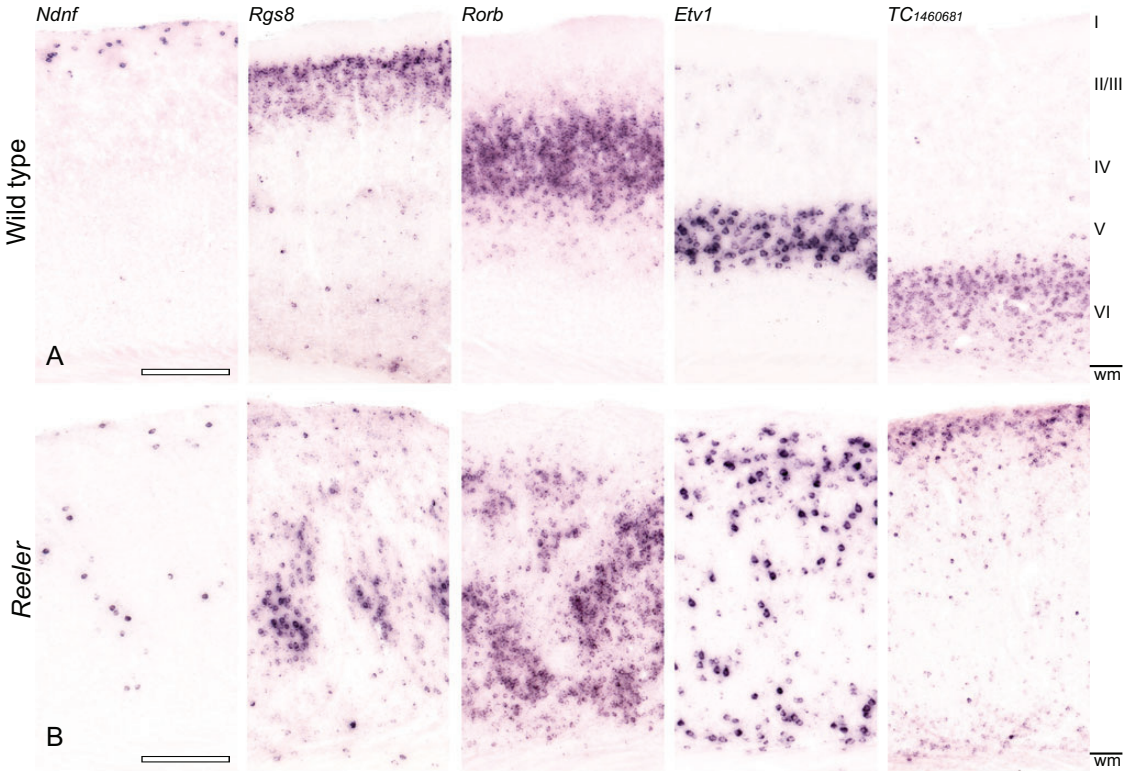

Figure 1. Layer-specific mRNA expression reveals a severely disrupted lamination of the *reeler* primary somatosensory (S1) cortex. Expression of *Ndnf* (L I), *Rgs8* (L II/III), *Rorb* (L IV), *Etv1* (L V), and *TC1460681* (L VI) were detected by NBT/BCIP chromogen RNA in situ hybridization in consecutive sections of the adult wild-type (*A*) and *reeler* (*B*) cortex. (*A*) In the wild-type brain, the markers reproduce the well-known lamination of the neocortex. (*B*) In the *reeler* cortex, however, the markers do not show obvious layers. Instead, a highly disordered pattern is displayed: *Ndnf*-positive neurons are scattered through the whole cortical column, clusters of *Rgs8*- and *Rorb*-positive neurons mainly inhabit a broad area in the middle of the cortex. These markers are flanked by loose bands of Etv1-, and TC1460681-positive neurons. Roman numerals indicate the wt layers; wm, white matter. Scale bars: 250 µm.

MBF Bioscience). The images were acquired as virtual tissues (VTs; 6 z-planes, 5-µm steps) and are presented as minimum intensity projections. To merge the laminar markers (Fig. 3), micrographs of consecutive sections were assigned to a respective false color and merged using Photoshop CS6 (Adobe). Fluorescent images (Figs 2, 4 and 5) were acquired using a spectral confocal microscope (TCS SP2, Leica). The Leica confocal software was controlled by the Vision4d software (Arivis) in order to acquire and stitch multiple, predefined tiles. Confocal micrographs are presented as maximum intensity projections.

Cell Counting and Statistical Analysis

Stimulated and unstimulated functional columns were delineated with Neurolucida and marker-labeled neurons with and without c-fos-positive nuclei registered manually within the outline. Data were exported with NeuroExplorer (MBF Bioscience) and exported in text files for Matlab R2010b import (MathWorks, MA, USA). We used a custom written script to display cells of 6 sections per condition in a single *n* by *m* array (Fig. 6E). For visualization of the activated neurons, a 150-pixel-wide Gaussian filter with a standard deviation of 12 pixels was applied to the array,

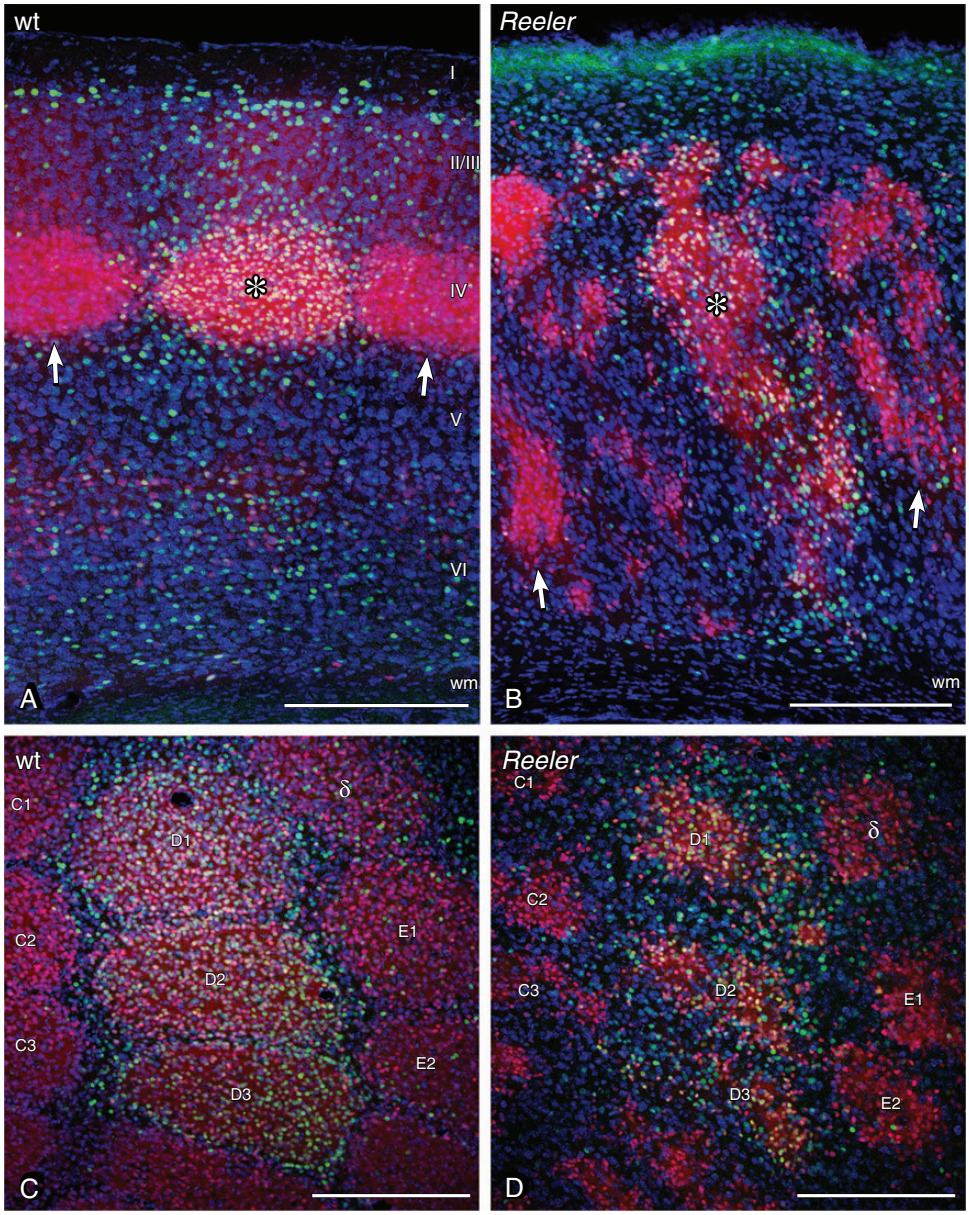

Figure 2. Neuronal activation in the barrel-related column of $LIV^{tdTomato}$ wild-type and *reeler* mice after tactile exploration of a novel, enriched environment. The whisker corresponding to stimulated columns were used during exploration, the whiskers corresponding to unstimulated columns were clipped before exploration. (*A*) Primary somatosensory (S1) cortex of wild type, sectioned in the coronal plane. The barrel as a layer IV structure becomes easily visible in the transgenic animal (red neurons). The stimulated wt column shows a substantially higher amount of c-fos-positive nuclei (green staining). The stimulated column is marked by a star within the barrel, and unstimulated columns are marked by arrows at the layer IV/V border. (*B*) S1 *reeler* cortex. Barrel equivalent patches are distributed over large parts of the cortex (red cells). However, the stimulated column again becomes visible by a higher amount of c-fos-positive nuclei. The stimulated column is marked by a star within one of the stimulated barrel equivalents, unstimulated columns are marked by arrows. Wild-type (*C*) and *reeler* (*D*) S1 barrel cortex sectioned in the tangential plane 400 µm below the pial surface. Barrels and barrel equivalents are labeled according to standard nomenclature. D1–D3 represent stimulated columns. Scale bars: 250 µm.

in order to obtain heat maps displaying the position of activated cell within the column (Fig. 6*H*,*I*).

The numbers/densities of the different excitatory and inhibitory neuronal populations, as well as the percentage of activated cells were analyzed with NeuroExplorer from reconstructed columns ($n = 6–8$ animals, 2 sections per animal for each condition). Data were exported to Excel (Microsoft) and statistical analysis was done using Sigma Plot 12 (systat). Significance was tested using two-tailed *t*-tests or Mann–Whitney rank-sum tests. The level of significance was set to $^{*}P < 0.05$; $^{**}P < 0.01$; $^{***}P < 0.001$.

Results

Intermingling of Different Laminar Marker-Labeled Neurons in the Disorganized Somatosensory *Reeler* Cortex

The organization of the *reeler* cortex has already been a subject of research for several decades (Meier and Hoag 1962; Caviness and Sidman 1973; Caviness et al. 1988). Recent work from our group as well as that of other groups strongly emphasized a complex cortical phenotype (Dekimoto et al. 2010; Wagener et al. 2010; Boyle et al. 2011; Pielecka-Fortuna et al. 2014).

This is in line with our present findings, based on layer-specific mRNA expression in the somatosensory cortex (Lein et al. 2007; Molyneaux et al. 2007). In the wild-type barrel cortex, the selected in situ markers labeled the layers I–VI with high sensitivity and specificity (Fig. 1*A*). In the corresponding region of the *reeler* cortex, no distinct layers became obvious after staining with the selected laminar markers (Fig. 1*B*): *Ndnf*-labeled neurons (layer I-marker) showed a random distribution throughout the whole barrel cortex, while *Rgs8*- (layer II/III-marker) and *Rorb*- (layer IV-marker) labeled neurons were predominantly located in the middle two thirds of the cortex. These neurons were sandwiched between *Etv1*- (layer V-marker) and *TC1460681*- (layer VI-marker) neurons, which were prevalent in the areas above the white matter and below the pial surface. However, it must be emphasized that this "sandwich" pattern is an oversimplification that does not take into account the fact that individual marker-labeled cells of any type could be found at virtually any depth of the cortex.

For preidentification of neurons with genetic layer IV characteristics which made them accessible to targeted electrophysiological recording, we crossed animals that expressed Cre-recombinase under a layer IV-specific promotor (*Scnn1a*) with our *reeler* strain and a suitable Cre reporter line (Madisen et al. 2010). Thus, we obtained wild-type and *reeler* animals that showed Cre-driven fluorescence (CDF) in layer IV and ectopic layer IV neurons (LIV^{tdTomato} mice) (Guy et al. 2015). The neurons showing CDF reproduced the pattern of *Rorb*-labeled layer IV neurons (Figs 1 vs. 2). The barrel, as a layer IV structure, became easily visible in the LIV^{tdTomato} wt animals (Fig. 2*A*,*C*). The equivalent clusters in the *reeler* cortex were called barrel equivalents (Wagener et al. 2010; Guy et al. 2015). They were smeared out over large parts of the cortical thickness, but still defined structural columns (Fig. 2*B*,*D*).

Behavioral Stimulation Activates Neurons That Form a Functional Column in the Disorganized *Reeler* Cortex

The responsiveness of the disorganized somatosensory *reeler* cortex was tested by challenging the animals with a naturalistic exploration task. To ease the read-out, we clipped the vibrissae of the animals and kept just a predefined set of whiskers (i.e., B1–3 and D1–3) with which the animals explored a novel, enriched environment (Staiger et al. 2000; Wagener et al. 2010). The nuclei of activated neurons were visualized by c-fos immunostaining. C-fos is, on the one hand, an immediate early gene that is activated within minutes after an adequate stimulus (Greenberg et al. 1985; Morgan and Curran 1989), but on the other hand, can be used as a metabolic marker of brain activity that provides single-cell resolution (Dragunow and Faull 1989; Staiger 2006). In the wild-type and *reeler* somatosensory cortex, the exploration specifically activated barrel-related columns that corresponded to whiskers that were used during the exploration task (stimulated column; Fig. 2*A*,*B*, asterisks; 2 *C*,*D*, barrels D1–3), while deprived columns (i.e., corresponding whiskers clipped) showed significantly fewer activated cells. Since these experiments were carried out in the LIV^{tdTomato} line, it became obvious that, in both genotypes, the activated nuclei could be found predominately in layer IV and ectopic layer IV neurons that showed CDF. These spiny layer IV neurons (Staiger et al. 2004) represent the main target of lemniscal thalamic fibers (Senft and Woolsey 1991; Oberlaender et al. 2012). To a lesser extent, activated neurons were distributed throughout the cortical column outside the CDF-positive compartment (i.e., barrels or "barrel equivalents"; Fig. 2).

Lemniscal TCAs and Laminar Affiliation of Potential Target Cells in the Barrel Cortex

Establishment of synaptic connections with layer IV target cells is an important prerequisite for intracolumnar processing of sensory information (Miller et al. 2001; Diamond et al. 2008). In both genotypes, the exploration task activated distinct neuronal ensembles, with a preference for CDF-positive layer IV and ectopic layer IV neurons. Thus, thalamic fibers might reach their layer IV target compartment even in the disorganized *reeler* cortex. In order to test this hypothesis, we traced lemniscal TCAs with an injection of a GFP-expressing viral vector (AAV2/6 eGFP) into the VPM of the thalamus. In the wild-type brain, the labeled TCAs made their way through the reticular nucleus into the internal capsule and the subcortical white matter before entering the cortex (Fig. 3*A*). Visualization of the potential cortical target layers by staining consecutive brain slides with the laminar markers revealed that TCAs preferentially target the hollow of the layer IV barrels (Fig. 3*C*, asterisks) and, to a lesser extent the layer V/VI border. This finding replicates and extends previous studies that were performed with different tracing techniques or species (Steindler and Colwell 1976; Caviness and Frost 1983; Wimmer et al. 2010). In the *reeler* cortex, the labeled TCAs followed a similar path (Fig. 3*B*) and entered the somatosensory cortex (Fig. 3*D*). There, a substantial number of TCAs formed thick bundles that made their way obliquely up to the pial surface before turning down again (Fig. 3*D*, arrows). The bundles defasciculated and the axons formed terminal fields that consisted of clustered patches of thin thalamic axons. Within these terminal fields, the TCAs joined with others that had not made the loop path from the white matter up to the pial surface. These observations go in line with previous descriptions in a reelin-deficient rat model (shaking rat Kawasaki), where a direct branching in the cortical plate was described to precede branching of the fibers that took the detour to the pial surface during developmental ingrowth of TCAs (Higashi et al. 2005).

The clusters of lemniscal axon terminals in the *reeler* cortex appeared to be as disorganized as the general cellular layout in the cortex. However, the axon clusters were shaped like the barrel equivalent clusters of ectopic layer IV cells and, indeed, lemniscal terminal fields overlapped, to a certain extent, with the clusters of *Rorb*-positive ectopic layer IV neurons in consecutive, marker-labeled brain sections (Fig. 3*D*, asterisks). No extensive overlap of

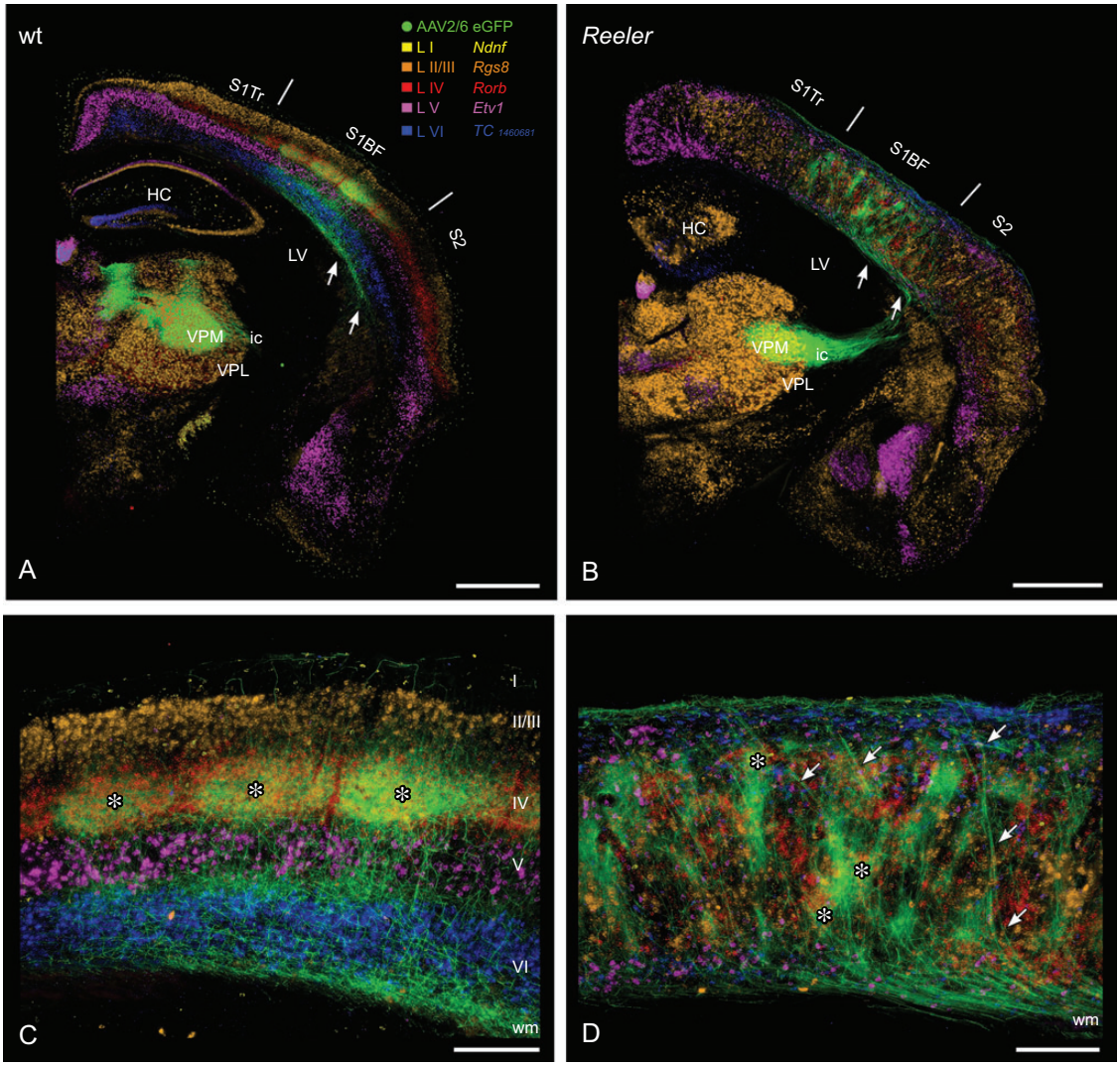

Figure 3. Lemniscal thalamic fibers and laminar affiliation of their potential cortical target cells in the wt and *reeler* primary somatosensory "barrel" cortex. Combination of anterograde viral tracing (AAV2/6 eGFP) of lemniscal thalamocortical axons (TCAs) and consecutive sections with chromogenic in situ hybridization for laminar markers (*A*, *B*) GFP-labeled TCAs from the ventral posteromedial thalamic nucleus reach the wild type (*A*) as well as the *reeler* cortex (*B*) via internal capsule and subcortical white matter (arrows). (*C*) In the wild-type cortex, thalamic terminal fields predominantly are concentrated in the barrel hollows of layer IV. Thus, they show a substantial overlap with the layer IV marker (*Rorb*, red). To a lesser extent, thalamic terminal fields can be found at the layer V/VI boarder. The barrels and there thalamic input are marked by asterisks. (*D*) In the disorganized *reeler* cortex, TCAs first run up to the pial surface, reverse and form terminal fields at different (vertical) levels of the cortex. These patches of thalamic axons in part overlap with the layer IV marker *Rorb* (asterisks). Laminar markers are presented in pseudocolors, they reproduce the pattern shown in Figure 1. HC, hippocampus; ic, internal capsule; LV, lateral ventricle; S1BF, barrel field; S2, secondary somatosensory cortex; S1Tr, primary somatosensory cortex, trunk region; VPL, ventral posterolateral thalamic nucleus; VPM, ventral posteromedial thalamic nucleus; wm, white matter. Scale bars: *A*, *B* 1000 µm; *C*, *D* 250 µm.

lemniscal terminal fields and other marker-labeled neuronal populations was obvious. It has to be taken into account that the applied method was restricted to visualization of the TCAs and to their potential cortical target cells in consecutive brain sections. Thus, specific targeting of thalamic fibers onto ectopic layer IV cells in the *reeler* cortex is suggested but not proven in this approach.

Optogenetic Stimulation of Lemniscal Thalamic Fibers Reveals Functional Synapses on Identified Ectopic Layer IV Cells

The tracing approach in the *reeler* brain potentially underscored the general capability of the thalamic fibers to target the disorganized somatosensory cortex. For a more fine-grained analysis of the targets of TCAs, including functional synaptic contacts, we made use of our LIV^{tdTomato} animals and combined optogenetic methods with patch-clamp slice electrophysiology. We performed stereotactic injections of a channelrhodopsin-expressing viral vector (AAV 2/6ChR2-eYFP) into the VPM of the thalamus (Fig. 4A,F). After an adequate expression time of the viral vector, acute brain slices were prepared. Putative layer IV neurons showing CDF in the wild-type and *reeler* cortex were patched and filled with biocytin for subsequent staining (Fig 4B,G). In the wild-type brain, membrane potential responses to somatic current application revealed regular spiking action potential firing patterns (Fig 4C). Thus, the responses are in line with the typical electrophysiological profile of layer IV spiny stellate neurons. The morphology of the biocytin-filled Alexa-labeled cells supported

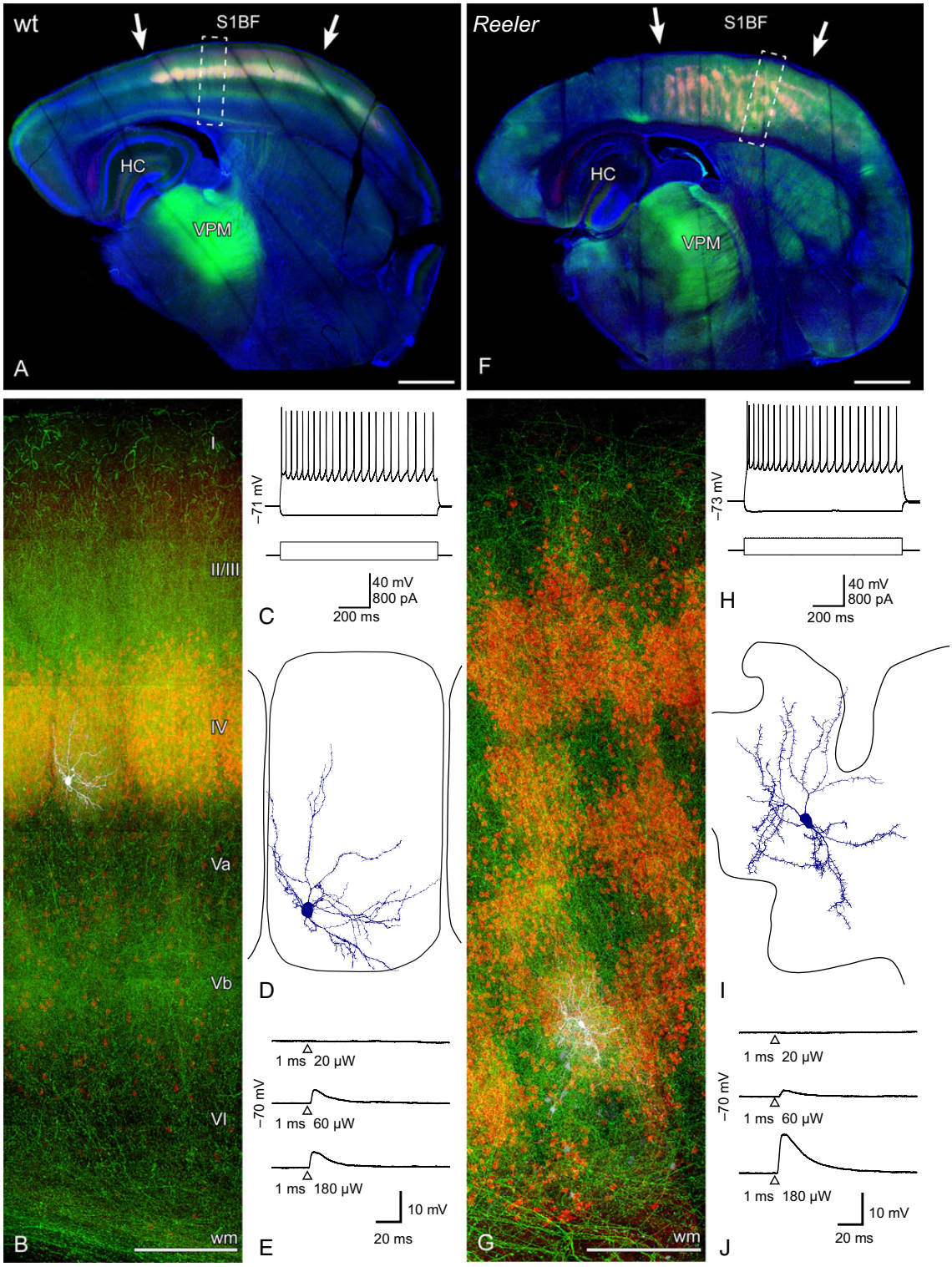

Figure 4. Photostimulation of ChR2-transduced thalamic projections to transgenically identified layer IV spiny stellate neurons of the barrel cortex. (*A*, *F*) Micrographs of the recorded slices of an AAV-injected (AAV2/6 ChR2-eYFP, green) wild-type (*A*) and *reeler* (*F*) $LIV^{tdtomato}$ (red) brain. The intense green spots in the thalamus represent the injection site in the ventral posteromedial thalamic nucleus (VPM). The dashed boxes indicate the functional columns that are shown in higher magnification below (*B*,*G*) and contain the recorded cell. (*B*, *G*) Maximum intensity projections of confocal image stacks of the patched tdTomato-positive neurons and their position in the functional column of the wild-type (*B*) and *reeler* (*G*) brain. The patched cells were filled with biocytin (visualized with streptavidin-Alexa 633, white). (*C*, *H*) Standard electrophysiological characterization shows the typical regular spiking (action potential) pattern of LIV spiny stellate neurons in wild type (*C*) and *reeler* (*H*). (*D*, *I*) Somatodendritic reconstructions of tdTomato-positive, biocytin-filled neurons. Note the restriction of the dendrites to the "home barrel" (wt; *D*) and "home barrel-equivalent" (*reeler*; I). (*E*, *J*) Examples of EPSPs evoked by photostimulation of ChR2-positive VPM axons with increasing intensities of a 473-nm laser. The time point of the laserflash is represented by a triangle below the trace. Note that the same amount of energy was needed to induce EPSPs in wild-type (*E*) and *reeler* (*J*) spiny stellates. HC, hippocampus; S1BF primary somatosensory barrel field; VPM, ventral posteromedial thalamic nucleus; wm, white matter. Scale bars: *A*, *F* 1000 µm; *B*, *G* 200 µm.

this notion (Fig. 4D): round to ellipsoid soma, absence of an apical dendrite, restriction of the dendrites to their "home barrel" and polarization of the dendrites toward the barrel center (Staiger et al. 2004). Flashes of blue laser light were able to evoke graded excitatory postsynaptic potentials (EPSPs) in all layer IV spiny stellate neurons tested ($n = 8$ from 3 different animals; Fig. 4E), with a latency that can be considered monosynaptic (mean ± SD latency: 1.693 ± 0.421 ms; cf., Kloc and Maffei 2014). Thus, the experimental setting was suitable to functionally verify lemniscal thalamic synapses on layer IV spiny stellate cells in the wild-type cortex.

In the disorganized *reeler* cortex, the same experimental procedure (i.e., patching a neuron showing CDF) again revealed a regular spiking pattern and the morphology of typical spiny stellate neurons (Fig. 4H,I) whose dendrites were restricted to the "home barrel equivalent." Moreover, stimulation of channelrhodopsin via laser flashes again reliably evoked EPSPs in all recorded CDF-positive neurons ($n = 9$ from 3 different animals; Fig. 4J) with a latency that indicates monosynaptic responses (mean ± SD latency: 2.131 ± 0.293 ms). The lowest laser power necessary to elicit EPSPs was not significantly different between the 2 genotypes (mean ± SD: wt 45.4 ± 36.3 µW; *reeler* 70.8 ± 48.2 µW; two-tailed, $P = 0.294$). Thus, despite the unusual pattern of the thalamic fibers and the pronounced disorganization of neurons showing CDF in *reeler*, the thalamic fibers established functional synaptic contacts onto the ectopic layer IV neurons.

Lemniscal Thalamic Fibers Specifically Target Clusters of Ectopic Layer IV Cells

The detected functional synaptic contacts between thalamic fibers and their native layer IV target cells must be considered necessary, but not sufficient for proper thalamocortical wiring. The reliably demonstrated functional contacts between lemniscal fibers and ectopic layer IV neurons showing CDF raise the question of the specificity of these contacts. In other words, do lemniscal TCAs in the disorganized cortex still preferentially target CDF-positive (layer IV) neurons, or has synapse formation become pervasive, and lemniscal synaptic connections are now formed without consideration to the laminar affiliation of target neurons? Our LIV^{tdTomato} animals together with viral tracing were helpful tools to answer this question. Injection of a GFP-expressing viral vector (AAV2/6 eGFP) into the VPM of LIV^{tdTomato} wild-type animals visualized the TCAs in great detail. The layer IV neurons within the barrels showed CDF of tdTomato (Fig. 5A). Simultaneous visualization of thalamic fibers and CDF confirmed their extensive overlap within the elliptically shaped wild-type barrel patch (Fig. 5C,C′,C″). To further verify synaptic contacts, we immunostained for vesicular glutamate transporter 2 (vGluT2; Fig. 5C‴), a marker that has been shown to predominately label lemniscal thalamic synapses (Graziano et al. 2008). The patch of marker-labeled putative lemniscal synapses matched the barrel as delineated by tdTomato-expressing layer IV neurons and GFP-expressing thalamic axons (Fig. 5C). Accordingly, the majority of the lemniscal TCA-synapses seem to be formed in this compartment of the wild-type cortex.

The same methods were used to investigate the potential targets of lemniscal TCAs in the disorganized *reeler* cortex (Fig. 5B). Several patches of neurons showing CDF within a functional column represented a barrel equivalent (Fig. 5B,D′) (Wagener et al. 2010). These patches were matched by thalamic terminal fields that accurately mimicked the shape and dimension of the barrel equivalents (Fig. 5D″). Furthermore, vGluT2 immunostaining for lemniscal thalamic synapses showed that these were formed preferentially within CDF-positive patches (Fig. 5D‴,D), making them truly barrel equivalent. Thus, despite the severe cortical intermingling of neurons with different laminar affiliations and the atypical pattern of TCAs, lemniscal synapses in the disorganized *reeler* cortex still seem to be predominately formed between lemniscal axons and ectopic layer IV neurons within barrel equivalent patches.

Distinct, Wild-Type Equivalent Excitatory and Inhibitory Neuronal Ensembles Participate in Behavioral Activation of the Disorganized *Reeler* Column

Wiring of thalamic efferents to layer IV cells is just the first step in the activation of the functional column (Petersen 2007). For further evaluation of the activation within the disorganized *reeler* column, we identified activated (c-fos-positive) excitatory and inhibitory neurons. Therefore, we combined our behavioral paradigm (i.e., exploration of an enriched environment with a defined whisker set) with immunostaining and ISH. A *Slc17a7* RNA probe was used for the identification of excitatory neurons (Fig. 6A,B). The distribution of excitatory cells within the column seemed to be different between the genotypes. In reconstructed wild-type columns, the cortical layers could be predicted by the density of excitatory neurons while *Slc17a7*-positive neurons in *reeler* columns were rather homogenously distributed (Fig. 6E). However, the density of excitatory cells within the whole column showed no significant statistical difference between the genotypes (Fig. 6F; Mann–Whitney rank sum, $P = 0.977$).

On a cellular level, c-fos-positive and c-fos-negative excitatory neurons could be identified in both genotypes (Fig. 6A′, B′; c-fos-positive excitatory cells marked by arrows, c-fos-negative neurons labeled by arrowheads). A higher amount of activated excitatory cells in both the wild-type and the disorganized *reeler* cortex defined stimulated columns (Fig. 6A,B; excitatory columns labeled with stars within the barrel/barrel equivalent, deprived columns labeled with asterisks). This effect was statistically significant in both genotypes (Fig. 6G; wt, two-tailed, $P = 0.0007$; *reeler*, two-tailed, $P = 0.012$). Moreover, the strength of the excitatory activation was the same in wild type and *reeler*, meaning that the percentage of activated neurons within a stimulated column was not significantly different between the genotypes (Fig. 6G; two-tailed, $P = 0.504$). The same was true for the comparison of deprived columns (Fig. 6G; two-tailed, $P = 0.256$).

Most of the activated excitatory neurons within the stimulated wild-type column were located in layer IV. This can be seen in individual columns (Fig. 2A) as well as in heat maps superimposing the location of activated excitatory neurons from 6 functional columns (Fig. 6H). Weaker spots of activation were located in layer II/III and in the upper part of layer VI. Because at least layer II/III neurons do not receive strong direct thalamic input (Fig. 5A), c-fos-positive neurons seem to partly reflect intracortical information processing. Individual stimulated functional *reeler* columns (Fig. 2B) as well as heat maps showing activated excitatory neurons in *reeler* ($n = 6$ columns; Fig. 6H), contained various spots of dense c-fos-positive neurons at different levels of the cortical depth (Figs 2B and 6H). These spots represent barrel equivalents. In addition, weaker spots of activation were distributed over the cortex, which again might reflect intracortical information processing.

For visualization of inhibitory neurons, a *Gad1* RNA probe was used (Fig. 6C,D). The distribution of inhibitory neurons in reconstructed wild-type columns did not clearly reproduce the cortical layers. Accordingly, the distribution of inhibitory neurons in the

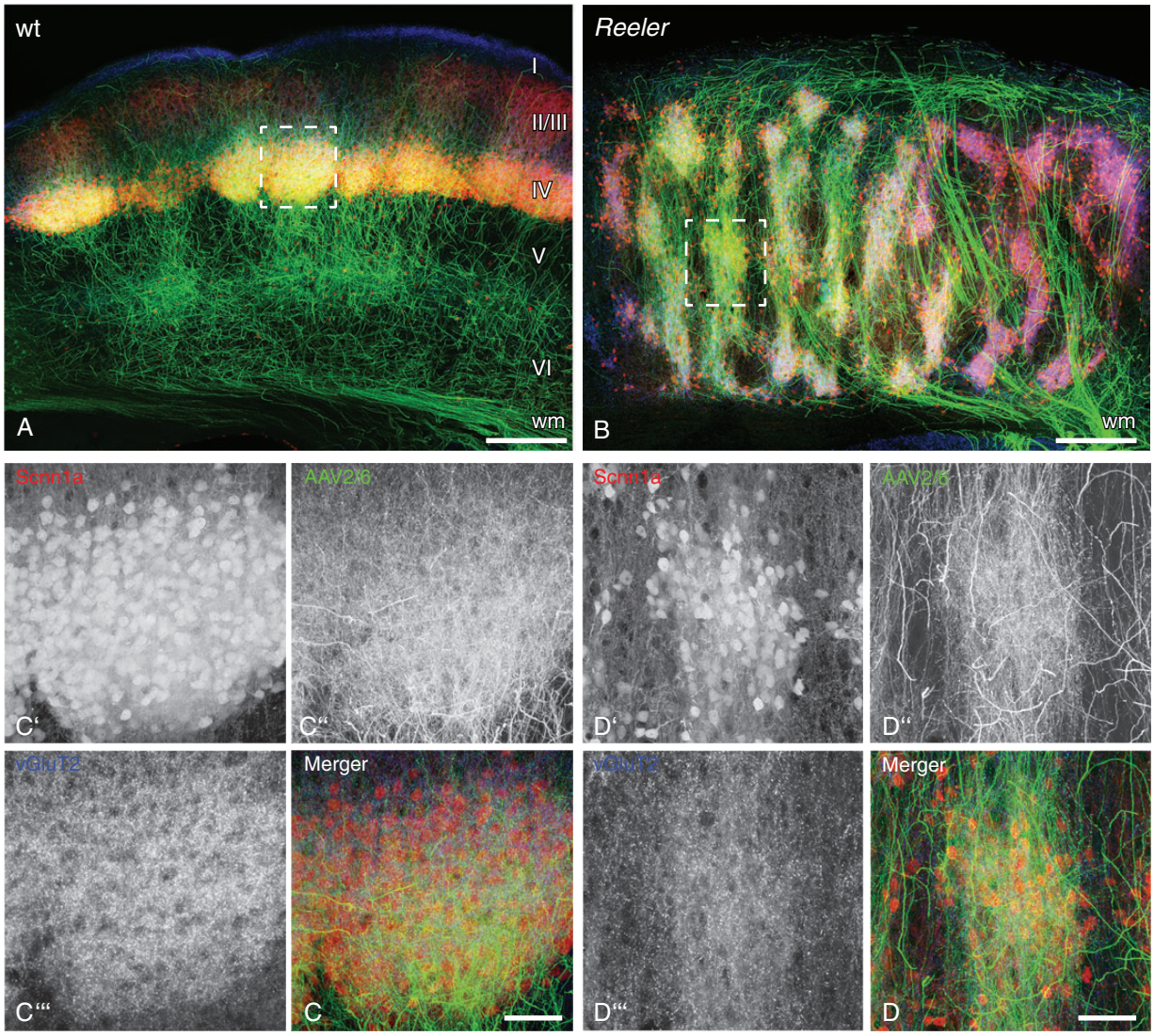

Figure 5. Thalamic fibers preferentially connect to tdTomato-positive neurons with genetic layer IV characteristics despite the severe vertical disorganization of the *reeler* primary somatosensory cortex. (*A*,*B*) Thalamic axons in the primary somatosensory barrel cortex after injection of GFP-expressing viral vector (AAV2/6 eGFP; green) into wild-type (*A*) and *reeler* (*B*) ventral posteromedial thalamic nucleus. tdTomato is expressed under the layer IV-specific Scnn1a promotor (red). (*C*,*D*) Higher magnification of a wild-type barrel (*C*) and *reeler* barrel equivalent (*D*) delineated by the dashed frames in the micrographs above (maximum intensity projection of 50 z-planes). (*C*′,*D*′) Single channel: tdTomato-positive cells; (*C*″,*D*″) Single channel: thalamic GFP-expressing axons; (*C*‴,*D*‴) Single channel: immunostaining for vGluT2, which labels lemniscal thalamic synapses. Note that the shape of thalamic terminal fields follows the distribution of tdTomato-positive cells in the wild-type (*C*) as well as the disorganized *reeler* column (*D*). Moreover, lemniscal synapses are concentrated in these overlapping spots, indicating that thalamic axons make specific synaptic contacts onto tdTomato-positive neurons with genetic layer IV affiliation. Scale bars: *A*, *B* 250 µm; *C*, *D* 50 µm.

wild-type and *reeler* column looked comparable, except for the presence of a higher number of cells close to the pial surface in the reeler (Fig. 6*E*). In the wild type, this location corresponds to cell-sparse layer I. Statistically, the number of inhibitory neurons in the *reeler* column was also comparable with that of wild-type cells (Fig. 6*F*; two-tailed, $P = 0.572$).

As with excitatory neurons, a higher amount of activated nuclei within the *Gad1*-positive neuron population defined stimulated functional columns (Fig. 6*C*,*D*). This effect again was statistically significant (Fig. 6*G*; wt, two-tailed, $P = 0.002$; *reeler*, two-tailed, $P = 0.008$). Moreover, the percentage of inhibitory neurons participating in the activation of the stimulated column was statistically similar between the 2 genotypes (Fig. 6*G*; two-tailed, $P = 0.620$). The same was true for deprived wild-type and *reeler* columns (Fig. 6*G*; two-tailed, $P = 0.451$).

Interestingly, hot spots of activated inhibitory neurons within stimulated wild-type columns showed a broad distribution, being present from layer II/III to layer Va. This again emphasizes the fact that the c-fos expression, at least partially, might be driven by intracolumnar activation (Fig. 6*I*). Moreover, the localization of activated inhibitory neurons could not be predicted by the general density of inhibitory neurons which appeared to be rather homogenously distributed along the column (Fig. 6*I*,*E*). Similar spots of activated inhibitory cells could be found in the *reeler* column (Fig. 6*I*). In accordance with the cellular architecture in *reeler*, these spots showed a wider vertical distribution throughout the cortex.

Altogether, the composition of excitatory and inhibitory cells participating in network activity of stimulated and deprived columns in the structurally disorganized *reeler* cortex was

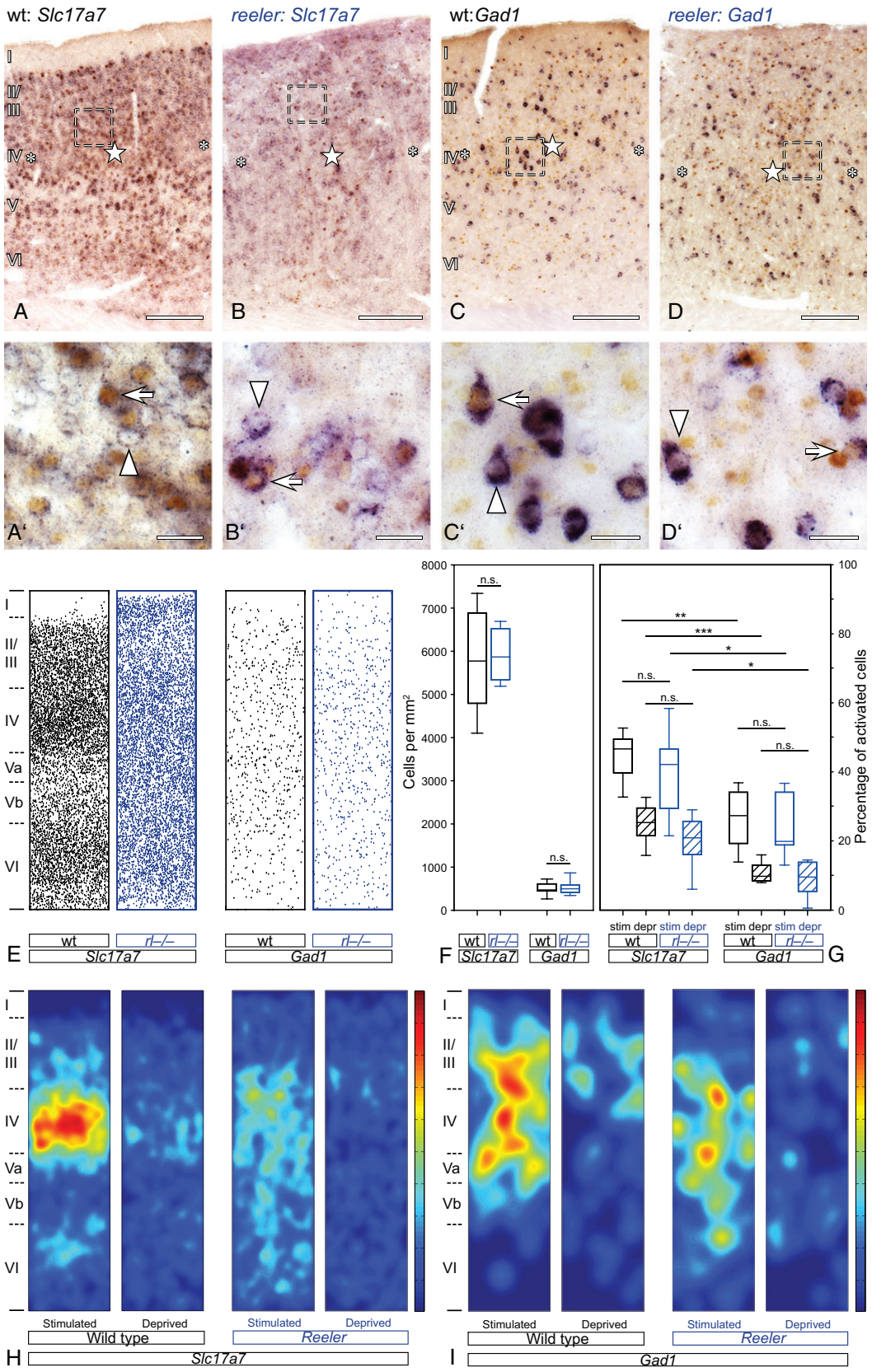

Figure 6. Activation of excitatory and inhibitory wild-type and *reeler* neurons after tactile exploration of a novel, enriched environment. (*A*–*D*) Stimulated and unstimulated barrel-related columns in the primary somatosensory "barrel" cortex. Excitatory (*Slc17a7*; *A*,*B*) or inhibitory (*Gad1*; *C*,*D*) neurons were labeled by chromogen RNA in situ hybridization (purple staining). Activated neurons were identified via immunostaining for the immediate early gene c-fos (DAB; brown staining of the nuclei). Stimulated columns are marked by a star in the wt barrel (*A*,*C*) or in *reeler* barrel equivalents, respectively. (*B*,*D*) Unstimulated columns are marked by asterisks. (*A*′–*D*′) The

surprisingly comparable with the wild-type condition. This finding becomes even more interesting when taking into account the fact that excitatory and inhibitory neuronal populations participated with individual and unique strengths in the activation (see below). A significantly higher percentage of excitatory neurons were activated by our behavioral paradigm (Fig. 6*G*; wt, two-tailed, $P = 0.002$). This difference between activated excitatory and inhibitory cells was statistically significant in *reeler* as well (Fig. 6*G*; *reeler*, two-tailed, $P = 0.039$).

Excitatory and Inhibitory Neuronal Subtypes Preserve Their Proportional Activation in the Disorganization *Reeler* Column

In order to achieve a more fine-grained analysis of activated neurons within the *reeler* column, we performed double immunolabeling of c-fos with markers for excitatory and inhibitory neuronal subpopulations (Fig. 7). There was no statistically significant difference in the density of neurons positive for the excitatory marker SMI32 in the wild-type and *reeler* functional columns (Fig. 7*A*,*E*,*I*; two-tailed, $P = 0.953$). The same held true for all inhibitory subpopulations tested: parvalbumin, calretinin, and calbindin (Fig. 7*B–D*, *F–H*, *I*; two-tailed, $P = 0.750$, 0.239, and 0.631). Moreover, all tested neuronal subpopulations showed a higher amount of activated (c-fos-positive) cells in stimulated columns compared with the deprived columns (Fig. 7*A–H*). This effect was always statistically significant in both genotypes (Fig. 7*J*; two-tailed, *P*-values: SMI32, Pvalb and CR wild type and *reeler*, all <0.001; Calb wt, 0.028; Calb *reeler*, 0.003). Thus, all neuronal subpopulations that were tested participated in the activation induced by the exploration task.

For each individual neuronal subpopulation, we could not detect any difference in the strength of the activation when comparing the wild-type and *reeler* columns. Neither stimulated nor deprived columns, showed statistically significant differences in the percentage of activated neurons (Fig. 7*J*; two-tailed, *P*-values: SMI32 stimulated, 0.458; SMI32 deprived, 0.478; Pvalb stimulated 0.184; Pvalb deprived 0.843; CR stimulated, 0.735; CR deprived 0.323; Calb stimulated, 0.689; Calb deprived, 0.394). However, the different neuronal subpopulations were activated with distinct strengths. The percentage of activated Pvalb-positive neurons in stimulated wild-type columns was significantly higher compared with the percentage of activated Calb-positive neurons in stimulated wild-type columns (Fig. 7*J*; two-tailed, $P = 0.017$), but was within the same range compared with CR-positive neurons (Fig. 7*J*; two-tailed, $P = 0.925$). CR-positive neurons in stimulated columns, in turn, showed a higher percentage of activated neurons compared with Calb-positive neurons (Fig. 7*J*; two-tailed, $P = 0.034$). Interestingly, the same conclusions were true for the neuronal subpopulations in activated *reeler* columns (Fig. 7*J*; two-tailed *P*-values: Pvalb vs. Calb, 0.004; Pvalb vs. CR, 0.354; CR vs. Calb, 0.01). Thus, the complex balance of excitatory and inhibitory neurons and neuronal subgroups that participated in columnar activation after behavioral stimulation was not impaired by the structural disorganization of the *reeler* column.

Discussion

In the present study, we demonstrate the preservation of basic principles of neuronal wiring and network activation in a brain with severely altered neocortical lamination. This holds true for long-range (i.e., thalamocortical) as well as short-range (i.e., intracortical) neuronal connections. We show targeting of ectopic layer IV neurons by lemniscal TCAs that resulted in functional synaptic contacts. Moreover, we found far-ranging similarities in intracortical activation patterns as the result of a behavioral task from which we conclude largely preserved intracortical wiring in the disorganized *reeler* brain.

Our study thus underscores the importance of genetic neuronal fate corresponding to time and place of neuronal origin over radial neuronal position. Neuronal fate seems to be the more important prerequisite for regular neuronal wiring and function (Hevner et al. 2003). In the *reeler* cortex, neurons misplaced due to migrational defects demonstrate the intrinsic ability to wire into functional networks even if they do not undergo synchronous migration with their laminar cohorts. Intrinsic transcriptional programs seem to compensate for the misplacement and ensure wiring into the appropriate network. These findings contradict the idea that cortical layers play a key role in enabling effective neuronal wiring and function in the sense of "good biological design" (Mitchison 1991; Cherniak 1995; Kaas 1997). Thus, cortical layering might represent a remnant of evolutionary remodeling, as it has been suggested for tangential cortical maps (Purves et al. 1992; Horton and Adams 2005).

The molecular mechanisms that underlie thalamocortical wiring, especially the final step in which thalamic fibers postnatally target layer IV cells, are little understood (Lopez-Bendito and Molnar 2003; Molnar et al. 2003). It is unclear if the laminar (radial) position of a neuron is important for the molecular mechanisms underlying the formation of terminal axonal arbors and finally synapse formation.

From our findings in the (radially) disorganized *reeler* cortex, we conclude that individual neurons, or at least individual ectopic neuronal clusters, are able to trigger the cascade of necessary molecular events. This speaks in favor of cell-autonomous molecular cues inducing synapse formation with the correct partners (Krishna-K et al. 2011; Carcea et al. 2014), rather than gradients established by the entire neuronal population of a layer.

Revisiting Thalamocortical Wiring in the *Reeler* Mouse

The idea of an inversion of neocortical layers in the *reeler* brain has been an attractive model to explain reelin function and has persisted in the literature for quite a long time (Caviness and Sidman 1973; Caviness 1982; D'Arcangelo 2005). Even if with time it became clear that the actual cortical phenotype has to be more

micrographs show a higher magnification of the area delineated by the dashed frames in *A–D*. Exclusively marker-labeled neurons are indicated by arrowheads, arrows point at marker-labeled neurons that show a c-fos-positive nucleus. (*E*) Distribution of excitatory and inhibitory neurons in reconstructed normalized columns. Each indicated column represents a superposition of functional columns from 6 individual sections. (*F*, *G*) Boxplots show the density of excitatory and inhibitory neurons (*F*) and the strength of the activation (*G*). Note that stimulated columns always show a higher amount of activated neurons and that the strength of activation is not significantly different between wild type and *reeler*. Bottom and top of the boxes represent the 25th and 75th percentiles, respectively; the bar in the box indicates the median. The ends of the whiskers represent the minimum or maximum, respectively. (*H*, *I*) Heat map represents the location of the activated nuclei within the functional column. Again, each displayed column represents a superposition of functional columns from 6 individual sections. Dark red indicates the highest density of activated neurons, and dark blue indicates the lowest. This value individually refers to the population of either excitatory or inhibitory neurons. Scale bars: *A–D* 200 µm; *A′–D′* 20 µm.

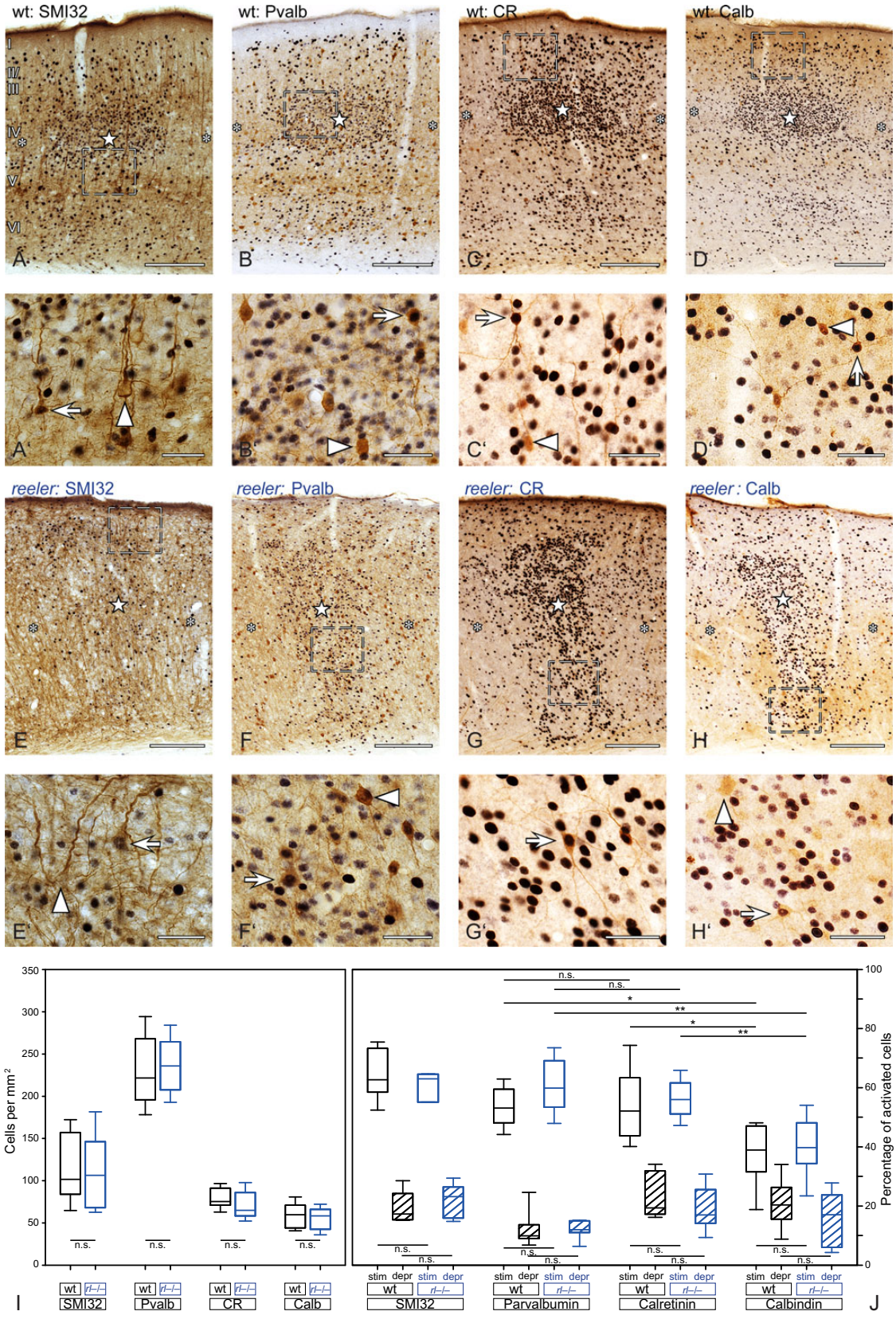

Figure 7. Activation of subgroups of excitatory and inhibitory wild-type and *reeler* neurons after tactile exploration of a novel, enriched environment. (*A*–*H*) Different subpopulation of excitatory and inhibitory neurons visualized by DAB immunostaining (brown). Nuclei of activated (c-fos-positive) neurons are revealed by DAB-Ni immunostaining (black). Stimulated columns are marked by a star within the wild-type barrel (*A*–*D*) or *reeler* barrel equivalent (*E*–*H*), and unstimulated columns are marked by asterisks. (*A*′*H*′) The micrographs show a higher magnification of the area delineated by the dashed frames in (*A*–*H*). Exclusively marker-labeled neurons

complex and disorganized (Welt and Steindler 1977; Rakic and Caviness 1995), the concept of "inverted layers" still is referred to in a number of recent publications. However, an increasing number of studies in the *reeler* brain could not be conciliated with this oversimplification, for example studies that examined the position of corticospinal projection neurons (Terashima et al. 1983; Polleux et al. 1998; Yamamoto et al. 2003). Recently, established molecular tools, such as layer-specific molecular makers (Molyneaux et al. 2007) and suitable transgenic animals (Madisen et al. 2010; Gerfen et al. 2013), have enabled us to reanalyze the cortical phenotype. The layer-specific markers used in the present study showed massive cellular intermingling, without revealing an inversion or well-distinguishable layers at all. However, it has to be mentioned that, at the level of subplate-specific genes, an expression pattern suggesting a layer-like compartmentalization has been described for the *reeler* cortex (Hoerder-Suabedissen et al. 2009; Oeschger et al. 2012).

The widespread distribution of molecularly identified neurons described in the present work confirms and substantially extends previous studies in which we demonstrated severe cellular intermingling in the *reeler* primary somatosensory cortex (Wagener et al. 2010) and primary visual cortex (Pielecka-Fortuna et al. 2014). These results were independently confirmed by other groups (Dekimoto et al. 2010; Boyle et al. 2011). The highly ectopic location of layer IV cells underscores the challenge thalamic fibers should have in targeting their native layer IV neurons.

Thalamocortical projections in *reeler* have been examined previously (Caviness 1976; Steindler and Colwell 1976; Caviness and Frost 1983). However, the studies lacked identification of presynaptic boutons on the axons as well as the postsynaptic layer IV target neurons. Furthermore, their interpretation was based on the idea of "inverted" cortical layers. Most of these studies supported the notion of intact thalamocortical pathfinding, but they also described the ingrowth of TCAs into a discernable layer IV being located in the deeper half of the cortex. However, based on the severely ectopic position of "layer IV" neurons as demonstrated in the present study with *Rorb* ISH and transgenic fluorescence labeling, these results are difficult to reconcile.

The ability to identify the native (layer IV) target population of TCAs (Molyneaux et al. 2007; Madisen et al. 2010) along with sophisticated viral vector based tracing methods (Luo et al. 2008; Wang et al. 2014) allowed us to reevaluate thalamocortical targeting in the *reeler* brain with unprecedented accuracy. Our results clearly show intact thalamocortical pathfinding and targeting of the newly revealed, highly ectopically positioned layer IV cells. Thus, thalamocortical synaptic contacts are formed between the correct partners, but distributed throughout the whole cortex. This finding is supported by work that has been done on the developmental organization of TCAs in the *reeler* cortex. The timing of the outgrowth of TCAs as well a transient synapse formation, important milestones of thalamocortical targeting, also showed extensive similarities to the wild-type developmental sequence (Yuasa et al. 1994; Molnar et al. 1998). Moreover, optical recordings with voltage-sensitive dyes in a rat model lacking reelin (shaking rat Kawasaki) support our finding (Higashi et al. 2005).

Further experiments on the ultrastructural and functional levels will be required in order to analyze more subtle changes in thalamocortical wiring. Array tomography and single fiber reconstruction could reveal changes in the number and dendritic location of thalamocortical synapses (Schoonover et al. 2014). Moreover, further electrophysiological functional analysis of the synaptic contacts could reveal more subtle functional deficits (Cruikshank et al. 2010; Kloc and Maffei 2014).

Functional Synapses in the Disorganized Cortex

The laminar marker results also demonstrated that, due to massive cellular intermingling, it is virtually impossible to identify a neuron of a specific laminar population in native sections of the *reeler* brain simply by its location. This might explain why very little electrophysiology has been done in the *reeler* brain (Drager 1981; Kowalski et al. 2010). In order to overcome this problem of identification, we crossed transgenic lines with our *reeler* strain. In the resulting LIV^{tdTomato} *reeler* line, a red fluorochrome was expressed under the layer IV-specific *Scnn1a* promotor (Madisen et al. 2010; Guy et al. 2015). Thus, CDF of ectopic layer IV neurons allowed for electrophysiological characterization of identified ectopic layer IV cells. Additional optogenetic photostimulation of lemniscal TCAs enabled us to functionally test adult thalamocortical synapses (Petreanu et al. 2007; Deisseroth 2011). We could demonstrate that the contacts between aberrant TCAs and ectopic layer IV cells indeed represent functional excitatory synapses, giving rise to graded EPSPs that should efficiently activate these neurons (cf. Cruikshank et al. 2010; Kloc and Maffei 2014), which seems to be key for the sensation of touch (Cruikshank et al. 2007; O'Connor et al. 2013).

Lessons Learned from Intact Wiring in the Vertically Disorganized Cortex (Protomap Theory)

Our finding of specific targeting of TCAs onto ectopic "layer IV" neurons speaks in favor of cell-autonomous molecular cues attracting the thalamic fibers. These apparently cell-intrinsic programs seem to not only preserve thalamocortical contact formation, but also retain columnar and thus tangential areal information. The mechanism mediating the ingrowth of thalamic fibers into the ectopic layer IV clusters could be mediated by the RAR-related orphan receptor beta (*Rorb*) which we demonstrate to be expressed in ectopic layer IV clusters of the *reeler* cortex. In the current study, *Rorb* mainly was used as a laminar marker, since it is strongly expressed in layer IV neurons (Schaeren-Wiemers et al. 1997). However, *Rorb* was shown to be expressed even before the ingrowth of thalamic fibers and peaks, during sharpening of tangential areal boarders. Moreover, ectopic expression of *Rorb* can induce the clustering of neurons and ingrowth of TCAs (Jabaudon et al. 2011). *Rorb* expression as an attractant of thalamic fibers even seems to be conserved across species (Belgard et al. 2013). Strong expression of *Rorb* as demonstrated in the adult *reeler* animals normally appears after the ingrowth of thalamic fibers (Nakagawa and O'Leary 2003).

The idea of ectopic layer IV neurons mediating thalamic ingrowth as well as formation of early tangential areal boarders (barrel formation) via *Rorb*, is in line with the protomap hypothesis. This model assigns the ability to build cortical maps to the individual neurons (Rakic 1988; Rakic et al. 2009). According to

are pointed at by arrowheads, and marker-labeled neurons that show a c-fos-positive nucleus are indicated by arrows. (*I*,*J*) Boxplots show the density of subgroups of excitatory and inhibitory neurons (*I*) and the strength of the activation (*J*). Note that stimulated columns always show a higher amount of activated neurons and that the strength of the activation is not significantly different between wild type and *reeler*. Bottom and top of the boxes represent the 25th and 75th percentiles, respectively; the bar in the box indicates the median. The ends of the whiskers represent the minimum or the maximum. Scale bars: *A*–*H* 200 µm; *A*′–*H*′ 40 µm.

the protomap model, the transcriptional fate, and thus the areal blueprint, is already determined at the time of the last neuronal division rather than by the ingrowth of thalamic fibers. We already could demonstrate functional tangential maps in the disorganized *reeler* cortex (Guy et al. 2015; Pielecka-Fortuna et al. 2014) and now can extend this finding by even demonstrating proper wiring within the radially disorganized cortical areas. This underlines the robustness of the cellular mechanisms controlling tangential arealization and wiring. Moreover, inclusion of radially dispersed neurons into tangentially organized networks indeed demonstrate that the capacity to establish map formation and wiring rather has to be assigned to individual cortical neurons, since *reeler* TCAs do not form a wild-type-like functional map at the position of a discrete layer IV. The predetermined fate of the ectopic layer IV neurons seems to guarantee inclusion in and establishment of the required neuronal networks. Based on our findings, arealization and ingrowth of thalamic fibers could be mediated by *Rorb* signals. The enhancement of the *Rorb* signal in the adult animal might reflect shaping and modification of the determined maps. This in part invokes the protocortex model that favors the idea of the strong influence of thalamic fibers in shaping the cortical maps (O'Leary 1989).

The idea that input from an orderly organized thalamus alone might not be sufficient to induce a wild type-like cortical barrel map also was found at the level of patterns of expression of developmentally regulated molecules in the *reeler* brain (Steindler et al. 1990). While brainstem and thalamus, in principle, develop normal in *reeler* (O'Brien et al. 1987), the expression pattern of adhesion and extracellular matrix molecules in the *reeler* barrel cortex showed disturbances (Steindler et al. 1990), which go in line with descriptions of disturbances at the cellular level (Welt and Steindler 1977; Wagener et al. 2010). In this context, the *reeler* model again supports the protomap theory, as it seems to be the TCAs deriving from an intact thalamus that adept to the ectopic position of disorganized cells. Moreover, the actual radial position of layer IV cells, as demonstrated in the present paper, might serve to interpret the altered distribution of adhesion molecules like cadherins (Steindler et al. 1990; Hertel and Redies 2011). There altered distribution might represent the plasticity necessary to established regular wiring in a structurally impaired cortex, again it has to be underlined that the tangential organization of cortical maps is preserved in this process (Welt and Steindler 1977; Guy et al. 2015).

Implications of Migration Defects on Neurologic and Psychiatric Diseases

The establishment of functional synapses after severe migration defects, even from long-range synaptic partners, is an especially interesting finding as there is an increasing number of neurological and psychiatric diseases for which a disturbance of neuronal migration is either suspected or has been demonstrated (Francis et al. 2006; Kerjan and Gleeson 2007; Mochida 2009; Valiente and Marin 2010). Our findings indicate that the phenotype of such diseases cannot necessarily be attributed to a considerably changed wiring as an effect of the migrational ectopy. In this context, it is interesting that besides its role as migrational regulator, reelin and its receptors also can influence synaptic transmission (Weeber et al. 2002; Hellwig et al. 2011). Taking into account the fact that fundamental wiring of the migrational disorganized *reeler* cortex can be compensated for by extensive developmental plasticity, synaptic impairment could be the mechanism of reelin deficiency with an even higher relevance for clinical symptoms. This could be an important starting point for the development of treatment strategies, because pharmacological modulation of synaptic transmission is a more common and promising approach than correction of migrational defects that have been described only in an experimental setting (Manent et al. 2009). However, it has to be recognized that most of the diseases that are related to migrational defects, including the loss of reelin, lead to further structural neurological pathologies than the mere disturbance of cortical neuronal positioning (D'Arcangelo 2005). Moreover, subtle pathophysiological effects, as a consequence of impaired neuronal and especially intracortical wiring, could have remained undetectable by our experimental approaches.

Altogether our results show that cellular composition, wiring, synapse formation, and functional columnar activation are strikingly "normal" for a neocortex with a severe vertical intermingling of neurons with different laminar affiliations and fates. Our study thus underscores the enormous developmental plasticity in the *reeler* cortex and argues for a rather insignificant role of vertical positional information compared with the compensatory capabilities of predetermined cell-intrinsic molecular programs.

Funding

This work has been funded through the Deutsche Forschungsgemeinschaft (DFG) Cluster of Excellence, Research Center "Nanoscale Microscopy and Molecular Physiology of the Brain" (J.F.S., Project area B1) and Sta 431/11-1. Funding to pay the Open Access publication charges for this article was provided by the University Medical Center Goettingen.

Notes

We thank Sandra Heinzl and Patricia Sprysch for excellent technical support. Thanks are due to Anna Dudek for expert technical assistance and proofreading. We also thank Rebecca Wallrafen for the acquisition of pictures for Figure 3 and Dr Martin Möck for interesting and helpful discussion of our results. *Conflict of Interest*: None declared.

References

Barth AL. 2007. Visualizing circuits and systems using transgenic reporters of neural activity. Curr Opin Neurobiol. 17:567–571.

Belgard TG, Montiel JF, Wang WZ, Garcia-Moreno F, Margulies EH, Ponting CP, Molnar Z. 2013. Adult pallium transcriptomes surprise in not reflecting predicted homologies across diverse chicken and mouse pallial sectors. Proc Natl Acad Sci USA. 110:13150–13155.

Bernardo KL, Woolsey TA. 1987. Axonal trajectories between mouse somatosensory thalamus and cortex. J Comp Neurol. 258:542–564.

Boyle MP, Bernard A, Thompson CL, Ng L, Boe A, Mortrud M, Hawrylycz MJ, Jones AR, Hevner RF, Lein ES. 2011. Cell-type-specific consequences of Reelin deficiency in the mouse neocortex, hippocampus, and amygdala. J Comp Neurol. 519:2061–2089.

Brecht M, Preilowski B, Merzenich MM. 1997. Functional architecture of the mystacial vibrissae. Behav Brain Res. 84:81–97.

Britto JM, Tait KJ, Johnston LA, Hammond VE, Kalloniatis M, Tan SS. 2011. Altered speeds and trajectories of neurons migrating in the ventricular and subventricular zones of the reeler neocortex. Cereb Cortex. 21:1018–1027.

Carcea I, Patil SB, Robison AJ, Mesias R, Huntsman MM, Froemke RC, Buxbaum JD, Huntley GW, Benson DL. 2014.

Maturation of cortical circuits requires Semaphorin 7A. Proc Natl Acad Sci USA. 111:13978–13983.
Caviness VS. 1982. Neocortical histogenesis in normal and reeler mice: a developmental study based upon [H-3] thymidin autoradiography. Dev Brain Res. 4:293–302.
Caviness VS. 1976. Patterns of cell and fiber distribution in the neocortex of the reeler mutant mouse. J Comp Neurol. 170:435–447.
Caviness VS Jr, Crandall JE, Edwards MA. 1988. The Reeler malformation: implications for neocortical histogenesis. In: Peters A, Jones E, editors. Cereb cortex. Vol. 7. New York: Plenum. p. 59–89.
Caviness VS, Frost DO. 1983. Thalamocortical projections in the reeler mutant mouse. J Comp Neurol. 219:182–202.
Caviness VS, Rakic P. 1978. Mechanisms of cortical development: a view from mutations in mice. Annu Rev Neurosci. 1:297–326.
Caviness VS, Sidman RL. 1973. Time of origin or corresponding cell classes in the cerebral cortex of normal and reeler mutant mice: an autoradiographic analysis. J Comp Neurol. 148:141–151.
Cherniak C. 1995. Neural component placement. Trends Neurosci. 18:522–527.
Cruikshank SJ, Lewis TJ, Connors BW. 2007. Synaptic basis for intense thalamocortical activation of feedforward inhibitory cells in neocortex. Nat Neurosci. 10:462–468.
Cruikshank SJ, Urabe H, Nurmikko AV, Connors BW. 2010. Pathway-specific feedforward circuits between thalamus and neocortex revealed by selective optical stimulation of axons. Neuron. 65:230–245.
D'Arcangelo G. 2005. The reeler mouse: anatomy of a mutant. Int Rev Neurobiol. 71:383–417.
Deisseroth K. 2011. Optogenetics. Nat Methods. 8:26–29.
Dekimoto H, Terashima T, Katsuyama Y. 2010. Dispersion of the neurons expressing layer specific markers in the reeler brain. Dev Growth Differ. 52:181–193.
Diamond ME, von Heimendahl M, Knutsen PM, Kleinfeld D, Ahissar E. 2008. 'Where' and 'what' in the whisker sensorimotor system. Nat Rev Neurosci. 9:601–612.
Drager UC. 1981. Observations on the organization of the visual-cortex in the reeler mouse. J Comp Neurol. 201:555–570.
Dragunow M, Faull R. 1989. The use of c-fos as a metabolic marker in neuronal pathway tracing. J Neurosci Meth. 29:261–265.
Francis F, Meyer G, Fallet-Bianco C, Moreno S, Kappeler C, Socorro AC, Tuy FPD, Beldjord C, Chelly J. 2006. Human disorders of cortical development: from past to present. Eur J Neurosci. 23:877–893.
Frost DO, Caviness VS. 1980. Radial organization of thalamic projections to the neocortex in the mouse. J Comp Neurol. 194: 369–393.
Gerfen CR, Paletzki R, Heintz N. 2013. GENSAT BAC cre-recombinase driver lines to study the functional organization of cerebral cortical and basal ganglia circuits. Neuron. 80:1368–1383.
Graziano A, Liu X-B, Murray KD, Jones EG. 2008. Vesicular glutamate transporters define two sets of glutamatergic afferents to the somatosensory thalamus and two thalamocortical projections in the mouse. J Comp Neurol. 507:1258–1276.
Greenberg ME, Greene LA, Ziff EB. 1985. Nerve growth factor and epidermal growth factor induce rapid transient changes in proto-oncogene transcription in PC12 cells. J Biol Chem. 260:14101–14110.
Grove E, Fukuchi-Shimogori T. 2003. Generating the cerebral cortical area map. Annu Rev Neurosci. 26:355–380.
Guic-Robles E, Valdivieso C, Guajardo G. 1989. Rats can learn a roughness discrimination using only their vibrissal system. Behav Brain Res. 31:285–289.
Guy J, Wagener RJ, Mock M, Staiger JF. 2015. Persistence of functional sensory maps in the absence of cortical layers in the somsatosensory cortex of reeler mice. Cereb Cortex. 25:2517–2528.
Harsan LA, David C, Reisert M, Schnell S, Hennig J, von Elverfeldt D, Staiger JF. 2013. Mapping remodeling of thalamocortical projections in the living reeler mouse brain by diffusion tractography. Proc Natl Acad Sci USA. 110: E1797–E1806.
Hashimoto-Torii K, Torii M, Sarkisian MR, Bartley CM, Shen J, Radtke F, Gridley T, Sestan N, Rakic P. 2008. Interaction between Reelin and Notch signaling regulates neuronal migration in the cerebral cortex. Neuron. 60:273–284.
Hellwig S, Hack I, Kowalski J, Brunne B, Jarowyj J, Unger A, Bock HH, Junghans D, Frotscher M. 2011. Role for reelin in neurotransmitter release. J Neurosci. 31:2352–2360.
Hertel N, Redies C. 2011. Absence of layer-specific cadherin expression profiles in the neocortex of the reeler mutant mouse. Cereb Cortex. 21:1105–1117.
Hevner R, Daza RA, Rubenstein JL, Stunnenberg H, Olavarria J, Englund C. 2003. Beyond laminar fate: toward a molecular classification of cortical projection/pyramidal neurons. Dev Neurosci. 25:139–151.
Higashi S, Hioki K, Kurotani T, Kasim N, Molnar Z. 2005. Functional thalamocortical synapse reorganization from subplate to layer IV during postnatal development in the reeler-like mutant rat (Shaking rat Kawasaki). J Neurosci. 25:1395–1406.
Hoerder-Suabedissen A, Wang WZ, Lee S, Davies KE, Goffinet AM, Rakic S, Parnavelas J, Reim K, Nicolic M, Paulsen O, et al. 2009. Novel markers reveal subpopulations of subplate neurons in the murine cerebral cortex. Cereb Cortex. 19:1738–1750.
Horton JC, Adams DL. 2005. The cortical column: a structure without a function. Philos Trans R Soc Lond B Biol Sci. 360:837–862.
Jabaudon D, Shnider SJ, Tischfield DJ, Galazo MJ, Macklis JD. 2011. RORbeta induces barrel-like neuronal clusters in the developing neocortex. Cereb Cortex. 22:996–1006.
Kaas JH. 1997. Topographic maps are fundamental to sensory processing. Brain Res Bull. 44:107–112.
Kerjan G, Gleeson JG. 2007. Genetic mechanisms underlying abnormal neuronal migration in classical lissencephaly. Trends Genet. 23:623–630.
Kleinfeld D, Deschenes M. 2011. Neuronal basis for object location in the vibrissa scanning sensorimotor system. Neuron. 72:455–468.
Kloc M, Maffei A. 2014. Target-specific properties of thalamocortical synapses onto layer 4 of mouse primary visual cortex. J Neurosci. 34:15455–15465.
Kowalski J, Geuting M, Paul S, Dieni S, Laurens J, Zhao S, Drakew A, Haas CA, Frotscher M, Vida I. 2010. Proper layering is important for precisely timed activation of hippocampal mossy cells. Cereb Cortex. 20:2043–2054.
Krishna-K K, Hertel N, Redies C. 2011. Cadherin expression in the somatosensory cortex: evidence for a combinatorial molecular code at the single-cell level. Neurosci. 175:37–48.
Lein ES, Hawrylycz MJ, Ao N, Ayres M, Bensinger A, Bernard A, Boe AF, Boguski MS, Brockway KS, Byrnes EJ, et al. 2007. Genome-wide atlas of gene expression in the adult mouse brain. Nature. 445:168–176.
Li H, Fertuzinhos S, Mohns E, Hnasko TS, Verhage M, Edwards R, Sestan N, Crair MC. 2013. Laminar and columnar development of barrel cortex relies on thalamocortical neurotransmission. Neuron. 79:970–986.
Lodato S, Rouaux C, Quast KB, Jantrachotechatchawan C, Studer M, Hensch TK, Arlotta P. 2011. Excitatory projection

neuron subtypes control the distribution of local inhibitory interneurons in the cerebral cortex. Neuron. 69:763–779.
Lopez-Bendito G, Molnar Z. 2003. Thalamocortical development: how are we going to get there? Nat Rev Neurosci. 4:276–289.
Luo L, Callaway EM, Svoboda K. 2008. Genetic dissection of neural circuits. Neuron. 57:634–660.
Madisen L, Zwingman TA, Sunkin SM, Oh SW, Zariwala HA, Gu H, Ng LL, Palmiter RD, Hawrylycz MJ, Jones AR, et al. 2010. A robust and high-throughput Cre reporting and characterization system for the whole mouse brain. Nat Neurosci. 13:133–140.
Manent JB, Wang Y, Chang Y, Paramasivam M, LoTurco JJ. 2009. Dcx reexpression reduces subcortical band heterotopia and seizure threshold in an animal model of neuronal migration disorder. Nat med. 15:84–90.
Meier H, Hoag WG. 1962. Neuropathology of reeler, a neuro-muscular mutation in mice. J Neuropath Exp Neur. 21:649–654.
Miller KD, Pinto DJ, Simons DJ. 2001. Processing in layer 4 of the neocortical circuit: new insights from visual and somatosensory cortex. Curr Opin Neurobiol. 11:488–497.
Mitchison G. 1991. Neuronal branching patterns and the economy of cortical wiring. Proc Biol Sci. 245:151–158.
Mochida GH. 2009. Genetics and biology of microcephaly and lissencephaly. Semin Pediatr Neurol. 16:120–126.
Molnar Z, Adams R, Goffinet AM, Blakemore C. 1998. The role of the first postmitotic cortical cells in the development of thalamocortical innervation in the reeler mouse. J Neurosci. 18:5746–5765.
Molnar Z, Garel S, Lopez-Bendito G, Maness P, Price DJ. 2012. Mechanisms controlling the guidance of thalamocortical axons through the embryonic forebrain. Eur J Neurosci. 35: 1573–1585.
Molnar Z, Higashi S, Lopez-Bendito G. 2003. Choreography of early thalamocortical development. Cereb Cortex. 13:661–669.
Molyneaux BJ, Arlotta P, Menezes JRL, Macklis JD. 2007. Neuronal subtype specification in the cerebral cortex. Nat Rev Neurosci. 8:427–437.
Morgan JI, Curran T. 1989. Stimulus-transcription coupling in neurons: role of cellular immediate-early genes. Trends Neurosci. 12:459–462.
Nakagawa Y, O'Leary DDM. 2003. Dynamic patterned expression of orphan nuclear receptor genes ROR alpha and ROR beta in developing mouse forebrain. Dev Neurosci. 25:234–244.
Oberlaender M, de Kock CP, Bruno RM, Ramirez A, Meyer HS, Dercksen VJ, Helmstaedter M, Sakmann B. 2012. Cell type-specific three-dimensional structure of thalamocortical circuits in a column of rat vibrissal cortex. Cereb Cortex. 22:2375–2391.
O'Brien TF, Steindler DA, Cooper NG. 1987. Abnormal glial and glycoconjugate dispositions in the somatosensory cortical barrel field of the early postnatal reeler mutant mouse. Brain Res. 429:309–317.
O'Connor DH, Hires SA, Guo ZCV, Li N, Yu JN, Sun QQ, Huber D, Svoboda K. 2013. Neural coding during active somatosensation revealed using illusory touch. Nat Neurosci. 16:958–965.
Oeschger FM, Wang WZ, Lee S, Garcia-Moreno F, Goffinet AM, Arbones ML, Rakic S, Molnar Z. 2012. Gene expression analysis of the embryonic subplate. Cereb Cortex. 22:1343–1359.
O'Leary DD. 1989. Do cortical areas emerge from a protocortex. Trends Neurosci. 12:400–406.
O'Leary DD, Nakagawa Y. 2002. Patterning centers, regulatory genes and extrinsic mechanisms controlling arealization of the neocortex. Curr Opin Neurobiol. 12:14–25.
Petersen CCH. 2007. The functional organization of the barrel cortex. Neuron. 56:339–355.
Petreanu L, Huber D, Sobczyk A, Svoboda K. 2007. Channelrhodopsin-2-assisted circuit mapping of long-range callosal projections. Nat Neurosci. 10:663–668.
Pielecka-Fortuna J, Wagener RJ, Martens AK, Goetze B, Schmidt KF, Staiger JF, Lowel S. 2014. The disorganized visual cortex in reelin-deficient mice is functional and allows for enhanced plasticity. Brain Struct Funct doi:10.1007/s00429–014–0866-x.
Polleux F, Dehay C, Kennedy H. 1998. Neurogenesis and commitment of corticospinal neurons in reeler. J Neurosci. 18: 9910–9923.
Purves D, Riddle DR, Lamantia AS. 1992. Iterated patterns of brain circuitry (or how the cortex gets its spots). Trends Neurosci. 15:362–368.
Rakic P. 1988. Specification of cerebral cortical areas. Science. 241:170–176.
Rakic P, Ayoub AE, Breunig JJ, Dominguez MH. 2009. Decision by division: making cortical maps. Trends Neurosci. 32:291–301.
Rakic P, Caviness VS. 1995. Cortical development: view from neurological mutants two decades later. Neuron. 14:1101–1104.
Sagar SM, Sharp FR, Curran T. 1988. Expression of c-Fos protein in brain-metabolic mapping at the cellular-level. Science. 240:1328–1341.
Schaeren-Wiemers N, André E, Kapfhammer JP, Becker-André M. 1997. The expression pattern of the orphan nuclear receptor RORbeta in the developing and adult rat nervous system suggests a role in the processing of sensory information and in circadian rhythm. Eur J Neurosci. 9:2687–2701.
Schoonover CE, Tapia JC, Schilling VC, Wimmer V, Blazeski R, Zhang W, Mason CA, Bruno RM. 2014. Comparative strength and dendritic organization of thalamocortical and corticocortical synapses onto excitatory layer 4 neurons. J Neurosci. 34:6746–6758.
Senft SL, Woolsey TA. 1991. Growth of thalamic afferents into mouse barrel cortex. Cereb Cortex. 1:308–335.
Staiger JF. 2006. Immediate-early gene expression in the barrel cortex. Somatosens Mot Res. 23:135–146.
Staiger JF, Bisler S, Schleicher A, Gass P, Stehle JH, Zilles K. 2000. Exploration of a novel environment leads to the expression of inducible transcription factors in barrel-related columns. Neuroscience. 99:7–16.
Staiger JF, Flagmeyer I, Schubert D, Zilles K, Kötter R, Luhmann HJ. 2004. Functional diversity of layer IV spiny neurons in rat somatosensory cortex: quantitative morphology of electrophysiologically characterized and biocytin labeled cells. Cereb Cortex. 14:690–701.
Staiger JF, Masanneck C, Bisler S, Schleicher A, Zuschratter W, Zilles K. 2002. Excitatory and inhibitory neurons express c-Fos in barrel-related columns after exploration of a novel environment. Neuroscience. 109:687–699.
Steindler DA, Colwell SA. 1976. Reeler mutant mouse: maintenance of appropriate and reciprocal connections in the cerebral cortex and thalamus. Brain Res. 113:386–393.
Steindler DA, Obrien TF, Laywell E, Harrington K, Faissner A, Schachner M. 1990. Boundaries during normal and abnormal brain-development—in vivo and in vitro studies of glia and glycoconjugates. Exp Neurol. 109:35–56.
Terashima T, Inoue K, Inoue Y, Mikoshiba K, Tsukada Y. 1983. Distribution and morphology of corticospinal tract neurons in reeler mouse cortex by the retrograd HRP method. J Comp Neurol. 218:190–205.
Valiente M, Marin O. 2010. Neuronal migration mechanisms in development and disease. Curr Opin Neurobiol. 20:68–78.
Wagener RJ, David C, Zhao ST, Haas CA, Staiger JF. 2010. The somatosensory cortex of reeler mutant mice shows absent

layering but intact formation and behavioral activation of columnar somatotopic maps. J Neurosci. 30:15700–15709.

Wang Q, Henry AM, Harris JA, Oh SW, Joines KM, Nyhus J, Hirokawa KE, Dee N, Mortrud M, Parry S, et al. 2014. Systematic comparison of adeno-associated virus and biotinylated dextran amine reveals equivalent sensitivity between tracers and novel projection targets in the mouse brain. J Comp Neurol. 522:1989–2012.

Weeber EJ, Beffert U, Jones C, Christian JM, Forster E, Sweatt JD, Herz J. 2002. Reelin and ApoE receptors cooperate to enhance hippocampal synaptic plasticity and learning. J Biol Chem. 277:39944–39952.

Welker C, Woolsey TA. 1974. Structure of layer IV in the somatosensory neocortex of the rat: description and comparison with the mouse. J Comp Neurol. 158:437–453.

Welt C, Steindler DA. 1977. Somatosensory cortical barrels and thalamic barreloids in reeler mutant mice. Neuroscience. 2:755–766.

Wimmer VC, Bruno RM, de Kock CP, Kuner T, Sakmann B. 2010. Dimensions of a projection column and architecture of VPM and POm axons in rat vibrissal cortex. Cereb Cortex. 20:2265–2276.

Woolsey TA, Van der Loos H. 1970. The structural organization of layer IV in the somatosensory region (SI) of mouse cerebral cortex. The description of a cortical field composed of discrete cytoarchitectonic units. Brain Res. 17:205–242.

Yamamoto T, Sakakibara S, Mikoshiba K, Terashima T. 2003. Ectopic corticospinal tract and corticothalamic tract neurons in the cerebral cortex of yotari and reeler mice. J Comp Neurol. 461:61–75.

Yassin L, Benedetti BL, Jouhanneau JS, Wen JA, Poulet JF, Barth AL. 2010. An embedded subnetwork of highly active neurons in the neocortex. Neuron. 68:1043–1050.

Yuasa S, Kitoh J, Kawamura K. 1994. Interactions between growing thalamocortical afferent axons and the neocortical primordium in normal and reeler mutant mice. Anat Embryol (Berl). 190:137–154.